Research Paper

Cytological and genetic consequences for the progeny of a mitotic catastrophe provoked by Topoisomerase II deficiency

Cristina Ramos-Pérez[1,2,6], Margaret Dominska[3], Laura Anaissi-Afonso[1,2], Sara Cazorla-Rivero[1,2], Oliver Quevedo[1,7], Isabel Lorenzo-Castrillejo[1], Thomas D. Petes[3], Félix Machín[1,4,5]

[1]Unidad de Investigación, Hospital Universitario Nuestra Señora de Candelaria, Santa Cruz de Tenerife, Spain
[2]Escuela de Doctorado y Estudios de Postgrado, Universidad de La Laguna, Tenerife, Spain
[3]Department of Molecular Genetics and Microbiology, Duke University Medical Center, Durham, NC 27710, USA
[4]Instituto de Tecnologías Biomédicas, Universidad de La Laguna, Tenerife, Spain
[5]Facultad de Ciencias de la Salud, Universidad Fernando Pessoa Canarias, Las Palmas de Gran Canaria, Spain
[6]Present address: BenchSci Analytics Inc., Toronto, Canada
[7]Present address: Genomic Integrity Unit, Danish Cancer Society Research Center, Copenhagen, Denmark

Correspondence to: Félix Machín, Thomas D. Petes; **email:** fmachin@funcanis.es, tom.petes@duke.edu
Keywords: mitotic catastrophe, Top2, senescence, cell death, genomic instability
Received: August 8, 2019 **Accepted:** November 24, 2019 **Published:** December 8, 2019

ABSTRACT

Topoisomerase II (Top2) removes topological linkages between replicated chromosomes. Top2 inhibition leads to mitotic catastrophe (MC) when cells unsuccessfully try to split their genetic material between the two daughter cells. Herein, we have characterized the fate of these daughter cells in the budding yeast. Clonogenic and microcolony experiments, in combination with vital and apoptotic stains, showed that 75% of daughter cells become senescent in the short term; they are unable to divide but remain alive. Decline in cell vitality then occurred, yet slowly, uncoordinatedly when comparing pairs of daughters, and independently of the cell death mediator Mca1/Yca1. Furthermore, we showed that senescence can be modulated by ploidy, suggesting that gross chromosome imbalances during segregation may account for this phenotype. Indeed, we found that diploid long-term survivors of the MC are prone to genomic imbalances such as trisomies, uniparental disomies and terminal loss of heterozygosity (LOH), the latter affecting the longest chromosome arms.

INTRODUCTION

Mitotic catastrophe (MC) is a class of cell death still poorly understood, and with a conflictive definition among the scientific community [1–3]. In its most general acceptation, we can consider MC as the cell-death-triggering event that follows an aberrant mitosis. MC is presumed to be of the utmost importance in cancer biology, both as an oncosuppressive barrier in carcinogenesis and as a mechanism of cell death after anti-cancer treatments. Many antitumor drugs that damage the DNA or the microtubules lead to chromosome segregation failures, provided that cells do not stop their division cycle in a timely fashion [4, 5]. Human cells make use of checkpoints to arrest the cell cycle in G_1/S or G_2/M following treatment with these antitumor drugs, and tumour cells frequently lack one or several of these checkpoints. When checkpoints are functional, cancer cells often die after a transient cell cycle arrest through a regulated cell death (RCD) known as intrinsic apoptosis [6]. Apoptosis causes the permeabilization of the mitochondrial outer membrane and the subsequent leakage of pro-apoptotic factors into the cytosol. Execution of the intrinsic apoptosis is significantly accelerated by the activation of the so-called caspase-mediated transduction cascade. When

checkpoints or apoptosis are non-functional, MC is expected to ensue. Therefore, understanding MC is becoming increasingly important in cancer biology.

MC is expected to kill most of the progeny due to major genomic imbalances and massive irreparable DNA damage. However, whether MC might also trigger a form of RCD or accidental cell death (ACD) is still unclear. In addition, MC is reported to lead to senescence in certain backgrounds [1, 7]. Senescence refers to the irreversible cell cycle arrest of otherwise live cells. Significant differences in the outcome are expected for MCs that result from different sources. Thus, MC occurring upon microtubule damage likely leads to missegregation of whole chromosomes prior to cell death, whereas DNA damage can give rise to more complex outcomes. For instance, DNA damage may result in either breakage of the DNA molecule (i.e, double strand breaks, DSBs) or replication stress (for example, stalled replication forks). Attempts to segregate broken chromosomes would yield daughter cells with irreparable damage. Attempts to segregate underreplicated chromosomes would cause the formation of anaphase bridges, which could produce DSBs as a consequence of cytokinesis [8–11]. Another condition that leads to MC concomitant with the appearance of anaphase bridges occurs when catenations between sister chromatids persist until anaphase. This happens when the catalytic action of topoisomerase II (Top2) is downregulated [12–14]. Top2 downregulation seems to pass undetected by cell cycle checkpoints in many cancer cell lines but not in normal differentiated cells [15–18]. Consequently, catalytic inhibition of Top2 offers a promising target to promote MC in cancer cells irrespective of the status of DNA damage checkpoints [19]. Of note, Top2 is often downregulated during acquisition of secondary resistance to chemotherapeutical regimes that comprise Top2 poisons, a major class of antitumor drugs [20, 21]. This observation implies that these resistant cancer cells should become even more hypersensitive to inhibition of Top2.

Top2 is essential in all organisms. In *Saccharomyces cerevisiae*, inactivation of Top2 by most thermosensitive (ts) alleles leads to MC in anaphase without previous checkpoint activation [13, 22–26]. In recent years, *S. cerevisiae* has also been a model to study both cell death pathways and genomic instability footprints after environmental or genetic insults [27, 28]. Here, we have characterized the consequences for the offspring of the MC that follows inactivating Top2 through the *top2-5* ts allele (hereafter refer to as *top2* MC). We show that most of the *top2* MC progeny lose their ability to divide. Interestingly, these daughter cells do not die abruptly but undergo a slow decline in cell vitality over several hours. The patterns of cell death point towards an ACD, which was genetically corroborated with mutants for the main apoptotic pathway. We have also used heterozygous diploids to diagnose chromosome rearrangements in the surviving progeny, and we found genomic footprints that include uniparental disomy and terminal loss of heterozygosity in the longest chromosome arms. We conclude that (i) most *top2* daughter cells become senescent in the short-term while eventually dying by ACD; and (ii) the surviving offspring frequently carry genomic rearrangements expected from transiting through anaphase with intertwined sister chromatids.

RESULTS

Seventy five percent of the progeny of a *top2-5* mitotic catastrophe is inviable

We have recently reported that the *top2-5* thermosensitive mutant undergoes timely progression through the cell cycle until a MC occurs in late anaphase [25]. Importantly, *top2-5* gives a clear point-of-no-return in the MC phenotype because cytokinesis makes the *top2-5* anaphase bridges collapse irreversibly. In many ways, this MC is similar to other previously studied *top2* conditional alleles [13, 24], although *top2-5* provides a better synchrony for the MC since a larger percentage of cells quickly sever the anaphase bridge [25].

We performed single-cell videomicroscopy on agar plates through long-range objectives and found that mother and daughter cells struggled to rebud (the most obvious yeast signal for a new cell cycle) without Top2 (Figure 1A) [25]. Whereas *TOP2* unbudded (G_1/G_0) cells were able to form microcolonies of around 10 cell bodies after 6 h at 37 °C, *top2-5* cells stopped dividing at either 2 (~65%) or 3 (~20%) cell bodies (Figure 1A). We hereafter refer to cell bodies rather than cells or buds since it is difficult to conclude whether a 3 cell-body is part of a single multi-budded cell, a budded mother with a daughter, or a mother with two daughters. This 2-3 cell-body pattern was an end-point phenotype upon continuous Top2 inactivation, since we observed the same proportions after 24 h at 37 °C (Figure 1B). Next, we investigated whether reactivation of Top2 by shifting the temperature down to 25 °C would allow any of these bodies to form a viable population. In order to have an overall picture of cell viability, we first determined clonogenic survival after different incubation periods at 37 °C. Because of the complexity of the budding patterns after the MC, we chose a solid medium-based clonogenic assay that allows to determine if at least one of the cell bodies was still viable by the time of the temperature shift, no matter how many cells are present in the

progeny (Figure 1C). We found that *top2-5* had a gradual loss of viability (50% survival after ~ 4 h), and less than 5% clonogenic survival was obtained after 24 h at 37 °C (Figure 1D); the *TOP2* isogenic strain retained the expected 100% clonogenic survival in this assay (Supplementary Figure 1A).

Because in these clonogenic assays there is a mixture of budded ($S/G_2/M$) and unbudded (G_1/G_0) cells at the time of plate seeding, we repeated the clonogenic survival after 6 h at 37° C, but photomicrographing the plate surface at different time points. Through this analysis, we determined that at time 0 h the unbudded:budded ratio was 2:1; however, only half of the surviving macrocolonies came from unbudded cells (Figure 1E). This result implies that the chance to become a macrocolony is doubled if the original cell was budded at the time of the temperature upshift. The

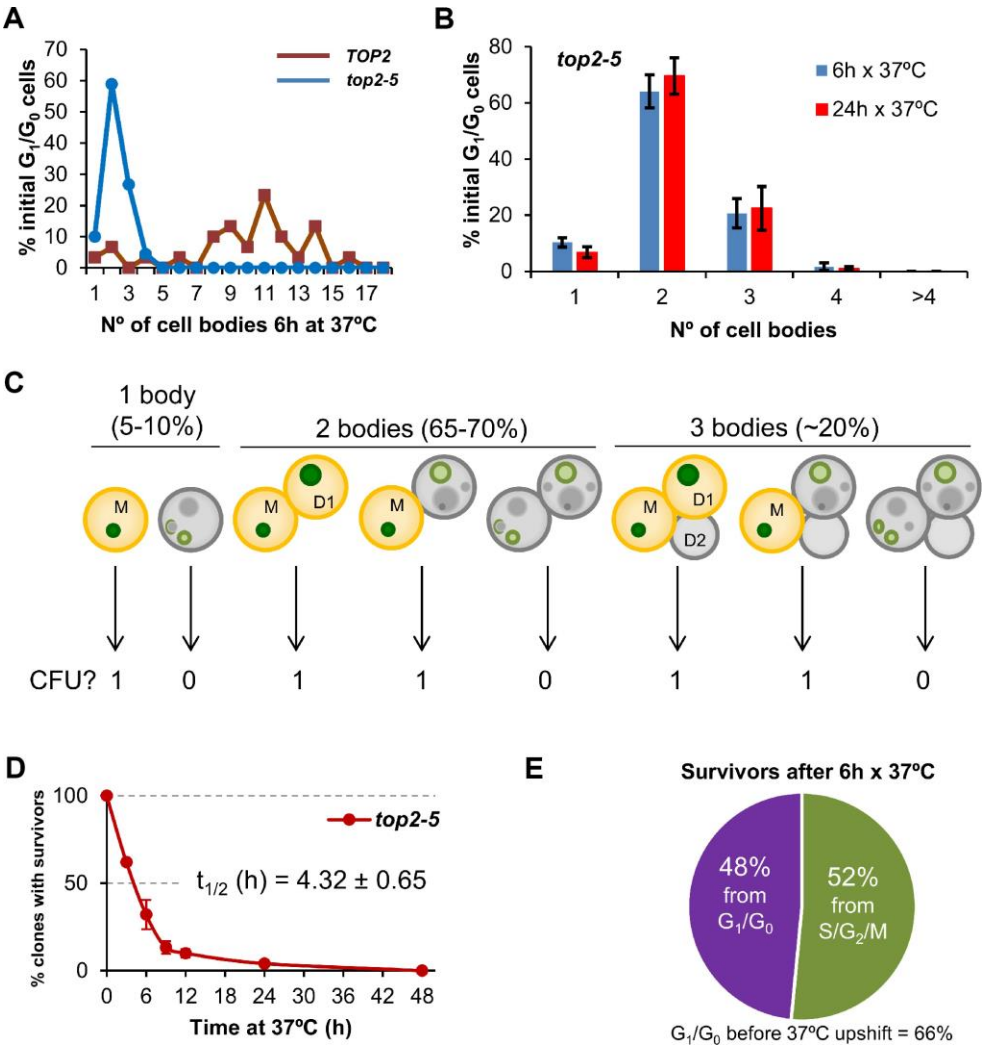

Figure 1. Most progeny coming from a Top2-mediated mitotic catastrophe is inviable. (**A**) Haploid *TOP2* (WT) or *top2-5* cells were grown at 25 °C and spread on YPD agar plates. Unbudded cells (G_1/G_0) were identified and photographed again after 6 h at 37 °C. Number of cell bodies (buds) coming from these G_1/G_0 cells were then counted and plotted as indicated. (**B**) The same analysis as in panel A but including data coming from independent experiments as well as after 24 h incubation at 37 °C (mean ± s.e.m., n=3). (**C**) The principle of the solid medium-based clonogenic assay. Unlike the liquid medium-based clonogenic assay, cells are spread on the Petri dish before the condition that challenges survivability is transiently triggered (Top2 inactivation in our study). In the solid medium-based assay, the colony forming unit (CFU) reading after the challenge is binary, irrespective of how far cells keep on dividing during the challenge: "0" if all clonal cells are inviable (grey); "1" if at least one cell from the clone stays viable (yellowish orange). (**D**) Time course of clonogenic survivability. Asynchronous *top2-5* cultures growing at 25 °C were spread onto several YPD plates. The plates were incubated at 37 °C for different periods before transferring them 25 °C. Four days after the initial plating, visible colonies (macrocolonies) were counted and normalized to a control plate which was never incubated at 37 °C (0h). (**E**) Analysis of the origin of macrocolonies after the 6 h x 37 °C regime as determined after microscanning plates at the time of seeding (N=33 macrocolonies; 2:1 unbudded:budded ratio at seeding).

most likely explanation for this bias resides in the fact that the *top2* MC is expected to be milder if cells are closer to anaphase onset when Top2 is inactivated. Indeed, budded cells appeared to better complete the first two cell cycles at the restrictive conditions (Supplementary Figure 2). A calculation based on the cell proportions at 0h (66% G_1/G_0; 33% $S/G_2/M$), overall macrocolony formation from the 37 °C for 6h regime (~25%), and the origin of those macrocolonies (~50% from G_1/G_0; ~50% from $S/G_2/M$) led us to conclude that around ~20% of the original G_1/G_0 cells gave rise to survivors after 6 h at 37 °C [0.25 × 0.5 / 0.66 = 0.19]. This proportion increases to ~40% for the $S/G_2/M$ cells at the time of the temperature upshift [0.25 × 0.5 / 0.33 = 0.38].

Most of the inviable progeny of a *top2-5* mitotic catastrophe immediately stops dividing

Next, we tried to correlate the long-term clonogenic survival of the G_1/G_0 cells with their ability to form microcolonies. We reasoned that it is possible that many MCs could render viable progeny in the short-term (microcolony) but could not raise a visible colony later (macrocolony). This difference could reflect a gradual loss of viability in the progeny as a consequence of genomic imbalances acquired after the MC. To get further insights into this possibility, we took pictures of the cells on the surface of Petri dishes at the time of seeding (0h), right after the 37 °C incubations (6h or 24h), and 16 h or 24 h after the plates were shifted back to 25 °C (Figure 2A). As expected from above, most of the original G_1/G_0 (unbudded) cells did not go beyond the 2-3 bodies stage during the 37 °C incubations (Figure 2A, 2B; inner circles in the sunburst plots). Restoring permissive conditions for Top2 activity allowed very few of the cell progeny to divide again (Figure 2A, 2B; outer circles in the sunburst plots). This finding was true not only during the long (24 h) incubation at 37 °C, but also for the 6 h incubation. Indeed, only ~15% of the 2-3 cell bodies observed after 6 h at 37 °C were able to re-bud again once or more after shifting them back to 25 °C. Incidentally, a low but significant proportion of G_1/G_0 cells did not bud during the 37 °C regimes. However, even in these non-MC cases, cells did not divide after the Top2 reactivation, suggesting that this G_1/G_0 subpopulation was already incapable of cell division following growth at 25 °C. Longer incubations at 25 °C after the MC resulted in microcolonies of >50 cells that eventually developed into macrocolonies. With our cell density settings, microcolonies of more than 20-30 cells hindered us from raising conclusions about the fate of adjacent cells. However, the position of the center in these microcolonies suggests that most, if not all, of the G_1/G_0 cells that ended up as macrocolonies had re-budded again within the first 24 h that followed the temperature downshift.

From previous analysis by videomicroscopy, we know that most *top2-5* doublets (2 bodies) and all triplets (3 bodies) have passed anaphase and thus completed a MC after 6 h at 37 °C [25]. Nevertheless, we decided to complete the analysis of the immediate progeny by testing whether the observed cell bodies have accomplished cell separation. Our reasoning was that separation by micromanipulation would demonstrate that cell bodies have become individual daughter cells. Indeed, we could separate with the needle more than half of the doublets and triplets (Figure 2C, middle concentric circle in the sunburst chart). We next tried to correlate the ability of all these cells to form macrocolonies but found that they were largely unviable. The percentage of macrocolonies (~2%) was much lower than expected, indicating that that micromanipulation killed cells that otherwise would have retained viability.

We noticed from the microcolony experiments performed above that cells swelled after prolonged incubations at 37 °C (Figure 2A). After 24 h at 37 °C, the volume occupied by the original mother cell doubled (Figure 2D). Downshift of the temperature to 25 °C only modestly deflated these cells. In addition, a low proportion of cell bodies underwent lysis ("0"; 2 → 1 and 3 → 2 categories in Figure 2B sunburst charts). These findings, together with the hypersensitivity to micromanipulation, led us to consider osmotic stress (due to the continuous growth in size of the mother cell) as a possible cause underlying the long-term inviability and/or short-term inability to divide of the *top2* progeny. However, addition of 1.2 M sorbitol, an osmotic stabilizer, neither prevented cells from swelling (Figure 2D) nor improved long-term viability (Figure 2E; Supplementary Figure 1B) or short-term division capability (Figure 2F; Supplementary Table 1).

Cell death after prolonged absence of Top2 activity occurs slowly, asynchronously, asymmetrically and is independent of the Yca1 metacaspase

Next, we analysed cell bodies in these microcolonies more closely, seeking other morphological patterns of cell disease aside from swelling; for example, lysis, darkening and loss of the rounded shape (Figure 3A). Most of these morphological features have been previously related to different forms of cell death. Because the *top2-5* strain also carries a GFP-labeled H2A histone, we also monitored nuclear morphology and chromatin integrity (i.e., GFP intensity). Cells still looked fully healthy after 6 h at 37 °C (no difference with 0 h), despite the great loss in the ability of the

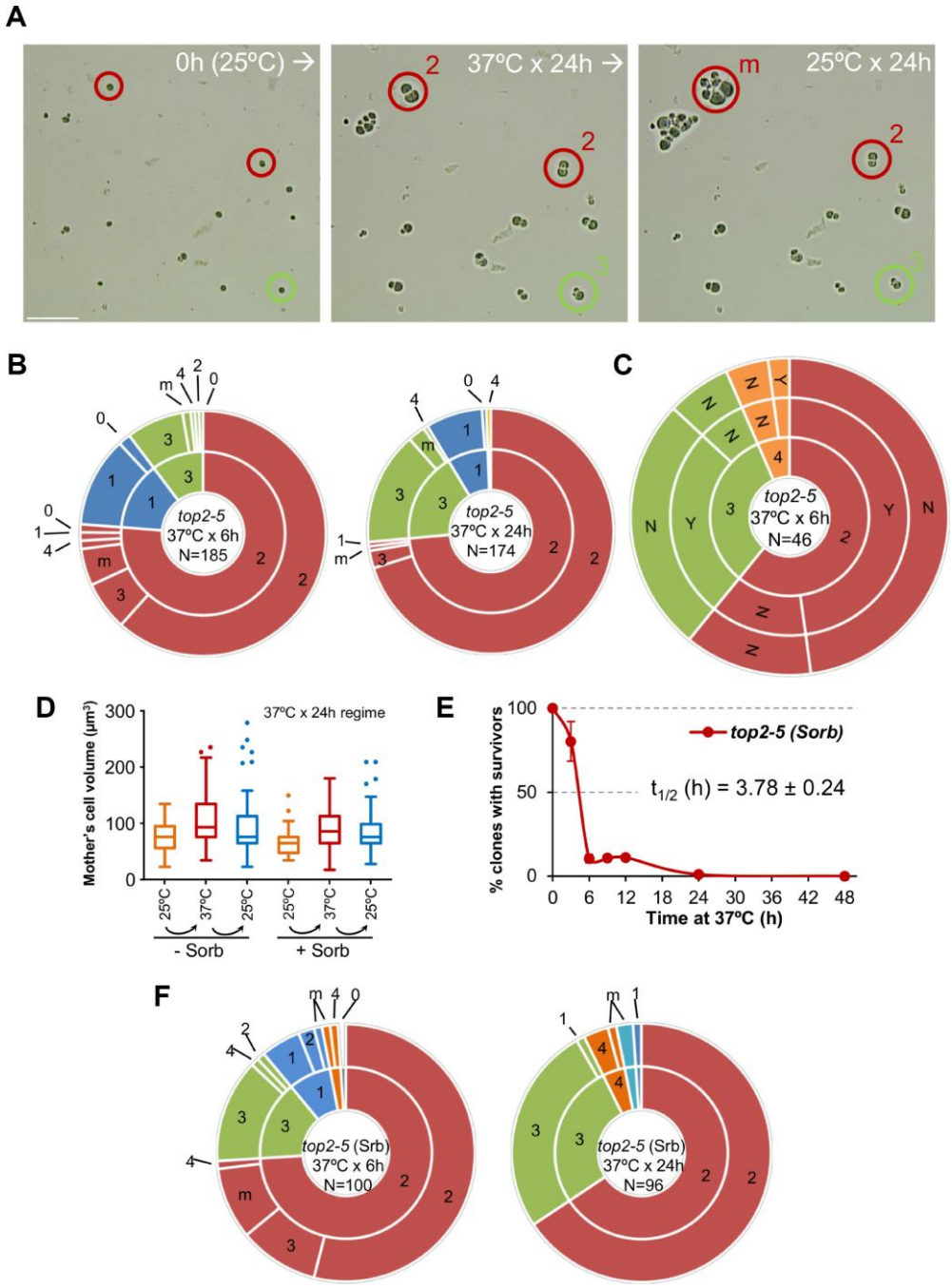

Figure 2. Most daughter cells coming from a Top2-mediated mitotic catastrophe are unable to divide again. (**A**) Haploid *top2-5* cells were spread at high cell density on two Petri dishes. At the time of seeding, 0h (25 °C), several fields were photomicrographed before incubating the plates at 37 °C during either 6 h or 24 h. After the 37 °C incubations, the same fields were localized, photomicrographed again, and further incubated 16-24 h at 25 °C. An example of a microscope field of a 37 °C x 24 h experiment. Three representative unbudded cells at 0h (25 °C) are highlighted. In red, two cells that budded just once during the 37 °C x 24 h incubation ("2" cell bodies); one of them able to re-bud again a few times after the 25 °C downshift ("m") and the second one that remained stuck as "2". In green, a cell that reached "3" bodies at 37° C and remained so after the final 25 °C x 24 h incubation. Scale bar corresponds to 50 µm. (**B**) Analysis of how far the *top2-5* MC progeny can go based on the microcolony approach shown in panel A. Only unbudded (G_1/G_0) cells at 0h (25 °C) were considered. The inner circle in the sunburst chart depicts proportions of cell bodies after the 37 °C incubation. The outer circle depicts the situation after the final 25 °C incubations (see supplemental information for a detailed description). On the left are results from a 37 °C x 6 h regime; on the right are results from a 37 °C x 24 h regime. Numbers point to the number of cell bodies; "m" means microcolonies of 5 or more bodies. (**C**) Capability of the *top2-5* progeny to split apart and relationship with overall survivability. Unbudded cells were micromanipulated and arranged at defined plate positions before incubating them for 6 h at 37 °C. Then, those cells able to re-bud at least once were subjected to an attempt to

physically separate the cell bodies. The inner circle in the sunburst depicts the number of cell bodies after the 37 °C incubation. The middle circle depicts the result of the separation attempt ("Y" or "N", successful or unsuccessful, respectively). The outer circle indicates if any of the bodies was able to raise a macrocolony (Yes or No) after 4 d incubation at 25 °C. (**D**) Progression of the size (volume) of the original G_1/G_0 cells (mother) after the *top2-5* mitotic catastrophe with and without the osmotic stabilizer Sorbitol (Sorb, 1.2 M). (**E**) Time course of clonogenic survivability in the presence of 1.2 M Sorbitol. The experiment was conducted as in Figure 1D. (**F**) Sunbursts of microcolony analyses in the presence of 1.2 M Sorbitol (Srb) at the 6 h and 24 h x 37 °C regimes. Interpretation as in panel B. In sunburst charts, N indicates number of original unbudded cells which were followed; blue sectors depict G_1/G_0 cells that remained unbudded during the 37 °C incubations; red sectors, cells that budded once at 37 °C; green sectors, cells that reached 3 bodies at 37 °C; orange sectors, cells that reached 4 bodies at 37 °C; cyan sectors, cells that reached 5 or more bodies at 37 °C.

progeny to divide. Only after prolonged 37 °C incubations did the cells start to look clearly sick. Still, more than 50% of cell bodies harboured a nuclear GFP signal even 24 h following the 37 °C upshift. This GFP signal co-existed in cell progenies that showed unhealthy patterns in the bright field such as swelled, darkened, or non-rounded cell bodies

In order to better study cell death after *top2* MC, we employed other means that required experiments to be performed in liquid media instead of Petri dishes. We first quantified the rate of cell death and metabolic decline by staining with the vital dye methylene blue (MB) (Figure 3B). This dye stains dead cells blue, although it can also stain cells that are alive but metabolically attenuated [29]. A time course after the 37 °C upshift showed that there was not a major increase in MB positive cell bodies in the first 4 h (the equivalent in liquid cultures to 6 h on solid medium; [25]). In general, the increase in MB+ bodies was linear, but even 24 h after the 37 °C upshift ~40% of cell bodies were not stained by MB. These staining experiments uncovered two other properties of the *top2* MC: i) it was common that only one cell body was MB+ in doublets and triplets (Supplementary Figure 3A); and ii) both unbudded and budded cells were equally stained (Supplementary Figure 3B). Regarding the first observation, the result suggests that loss of vitality is not coordinated between mother and daughter(s) cells. This asymmetry also confirms that many doublets must have completed cytokinesis despite remaining together. As for the second observation, the staining pattern suggests that loss of vitality occurs in an asynchronous fashion in terms of any preference for a cell cycle stage.

Because MB does not distinguish whether cell bodies are dead or simply metabolically stressed, we next sought other more informative vital stains. First, we employed the fluorescent vitality probe FUN1©. This probe stains metabolically active live cells with red vacuolar aggregates [30]. FUN1© is considered more informative and reliable than MB. With this probe we confirmed that only ~10% of cell bodies have lost vitality after just 4 h at 37 °C (left chart of Figure 3C; Supplementary Figure 4). It was also surprising that vitality decline still affected no more than 40% of all cell bodies after 24 h at 37 °C.

We also used Propidium Iodide (PI) to monitor cell viability. Loss of plasma membrane impermeability is considered a *bona fide* marker of cell death [27]. PI is only able to fluorescently stain cells that have lost such impermeability. Anticipating some sort of RCD after the *top2* MC, we decided to accompany PI staining in red with reporters for either reactive oxygen species (ROS) or externalization of phosphatidylserine (PS) at the plasma membrane; both in green (DCFH-DA and annexinV-FITC, respectively). Intrinsic ROS production has been observed during RCD in all eukaryotes, including yeast, and is considered one of most reliable RCD markers [31]. After overnight growth at 25 °C (0h), the *top2-5* strain had neither dead cells nor cells with ROS (right part of Figure 3C, Supplementary Figure 5). Four hours after the 37 °C temperature shift, there was only a slight increase in dead cell bodies (~6%) and almost no signs of ROS in the rest (~3%). Only after 24 h of incubating the cells at 37 °C, we found a significant proportion of both ROS (~20%) and dead cells (~20%). It is noteworthy that the percentage of PI+ cells was still relatively low after this 24 h incubation, and 60% of all cell bodies were still resistant to PI and free of ROS. Similarly, PS externalization is considered a conserved *bona fide* marker of RCD [32]. Double staining with PI and annexin V-FITC in cells where the cell wall has been digested (a necessary step for annexin V to reach externalized PS) showed less than 10% of cell bodies with the staining expected for early apoptosis, even 24 h after the temperature upshift (Supplementary Figure 6; annexin V positive plus PI negative). It is noteworthy that there were more dead cell bodies (PI positive) in this assay than in the ROS/PI assay (~60% vs. ~20%). This observation is likely a consequence of digesting the cell wall, since the plasma membrane of swollen cells at 24 h might collapse during the treatment.

We next examined if the observed pattern of death after the *top2* MC was altered by a mutation in caspase. We reasoned that this approach might shed more light on

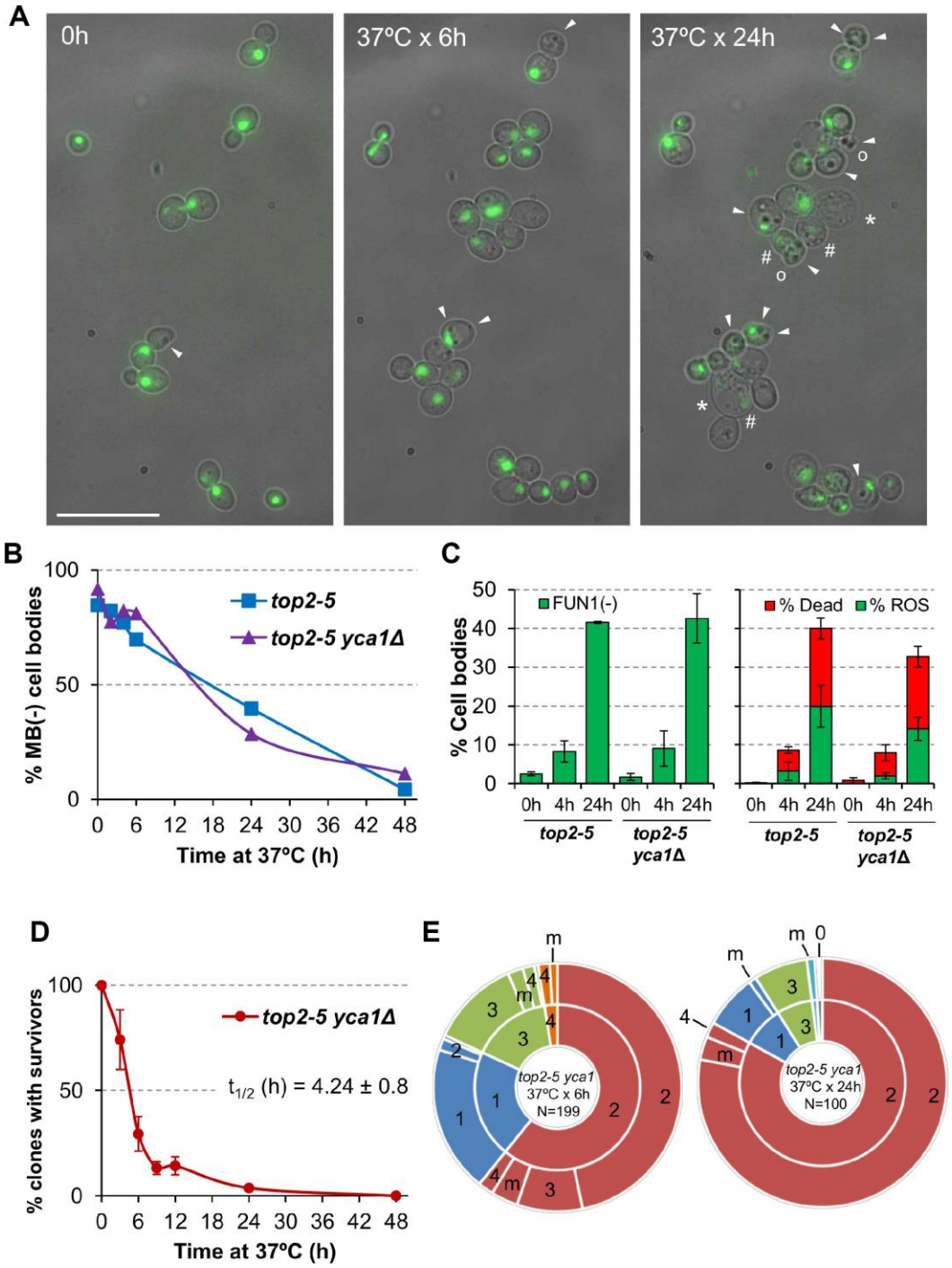

Figure 3. Cell vitality remain high for several hours after the *top2* mitotic catastrophe and is not modulated by Yca1. (**A**) Morphological patterns of cell and nuclear sickness after the *top2* MC. Haploid *top2-5 HTA2-GFP* cells were seeded onto agarose patches and the same fields visualized under the fluorescence microscope at 0 h, 6 h and 24 h after the 37 °C temperature upshift. White filled triangles point to darkened inclusion bodies, asterisks (*) swelled cells, open circles (○) cells that has lost their rounded shape, and hash (#) points to cells that have largely lost the H2A-GFP signal. BF, bright field. Scale bar corresponds to 20 µm. (**B**) Time course of cell vitality decline as reporter by methylene blue (MB) negative staining. Asynchronous cultures of the *top2-5* and *top2-5 yca1*Δ strains were grown at 25 °C before shifting the temperature to 37 °C. At the indicated time points (0, 2, 4, 6, 24 & 48 h), samples were taken and stained with the vital dye MB. (**C**) Cell vitality decline as reported by metabolic competence, intrinsic ROS generation, and loss of plasma membrane impermeability. Cells were treated as in B and stained at the indicated time points with the vital dye FUN1, the death marker propidium iodide (PI), and/or the ROS reporter DCFH-DA (mean ± s.e.m., n=3). (**D**) Clonogenic survival profile of *top2-5 yca1*Δ as determined on the low-density plates (mean ± s.e.m., n=3). The experimental procedure is described in Figure 1D. (**E**) Ability to re-bud of the *top2-5 yca1*Δ MC progeny as determined on the high-density plates. The experimental procedure is described in Figure 2.

the RCD/ACD nature of the observed death, considering the low presence of intrinsic ROS and the technical caveats of the annexin V assay. Hence, we deleted the only caspase-like gene in yeast, *YCA1/MCA1*. Yca1 is required for RCD in yeast in response to several environmental stresses [33–35]. In addition to cell death, we checked whether Yca1 modulated the other behaviours seen in the *top2* MC progeny (for example, the inability to divide and the slow decline in cell vitality). The conclusions derived from comparing *top2-5 YCA1* and *top2-5 yca1*Δ were that Yca1/Mca1: (i) had no influence in the percentage or rate of cells that end up dying (Figure 3B, 3C); (ii) neither accelerated nor slowed down the vitality decline (Figure 3B, 3C); (iii) did not modify the profile of clonogenic survival after the *top2* MC (Figure 3D; Supplementary Figure 1C); and (iv) its absence did not improve the ability of the immediate cell progeny to divide (Figure 3E; Supplementary Table 1).

The overall conclusion from these experiments is that the immediate progeny of the *top2* MC enter a senescent-like state as they retain vitality but loses their ability to re-bud. Senescence is only a transient state that lasts several hours or days, until cells eventually die. The pattern of cell death (morphologically diverse, slow, asynchronous and asymmetrical), together with the lack of effect of Yca1, suggest that loss of Top2 leads to ACD.

Chromosome ploidy modulates the ability of the progeny to divide

All the experiments described above were carried out in haploid yeast cells. In haploids, MC associated with the presence of partly unresolved sister chromatids, as in the *top2-5* mutant, is expected to be highly deleterious. Severing of these anaphase bridges result in daughter cells that may lack several chromosome arms [11]. Based on this consideration, one might expect that diploid cells would be more resistant to the consequences of *top2* MC than haploid cells. Thus, we studied the *top2* MC in an isogenic homozygous *top2-5/top2-5* diploid (2N) strain. Unlike its haploid counterparts, diploid cells were more often able to re-bud at least once. In fact, ~50% of all 2-3 cell bodies originated from just after 6h at 37 °C were able to do so after the 25 °C downshift (Figure 4A; Supplementary Table 1). This percentage dropped considerably if the progeny was incubated 24 h at 37 °C. Strikingly, however, the increase in the ability to divide again after the MC did not yield better clonogenic survival (Figure 4B; Supplementary Figure 1D), indicating that most of this viable progeny was competent to re-bud only in the first generations. We also performed a microdissection analysis of the diploid *top2* progeny. Unlike haploid *top2-5* cells, which was rather sensitive to micromanipulation, 13% of the diploid progeny raised a macrocolony after the separation attempt (Figure 4C). Altogether, we conclude that a *top2* MC in diploids results in better short-term ability to divide.

Genome instability footprints in the surviving progeny from the *top2*-mediated mitotic catastrophe

Above, we have just shown that ~25% of the *top2-5* diploid cells still gave rise a macrocolony after the 6h at 37°C regime. We next examined the genomes of these survivors in search for specific genomic footprints of the *top2* MC. To accomplish this goal, instead of using the homozygous isogenic diploid employed in the previous chapter, we generated a highly heterozygous hybrid *top2-5* diploid. The hybrid diploid was generated by crosses of two sequence-diverged *top2-5* haploids, derivatives of W303-1A and YJM789, which are heterozygous for more than 55,000 single-nucleotide polymorphisms (SNPs) distributed throughout the yeast genome (the yeast genome is 15 Mb). These heterozygous SNPs allow the analysis of various types of genomic alterations by using SNP-specific microarrays [36, 37]. The hybrid diploid is also engineered to select various types of chromosome alterations on chromosome V (Figure 5A). It is homozygous for the *ade2-1* mutation on chromosome XV (an ochre-suppressible allele) and heterozygous for the *SUP4-o* suppressor gene in chromosome V [38]. Strains with the *ade2-1* mutation form red colonies in YPD in the absence of the *SUP4-o* suppressor. Diploid strains with one or two copies of *SUP4-o* form pink and white colonies, respectively [39]. Thus, loss of the *SUP4-o* gene by either mitotic recombination or chromosome loss results in a red colony instead of the pink colonies characteristic of the original strain. Colony colour changes are also expected if the copy number of the *ade2-1* allele varies by loss or duplication of chromosome XV. In addition, aneuploidy for other chromosomes sometimes alters the color of the colony.

Microcolony and clonogenic experiments performed in the *top2-5* hybrid diploid FM1873 showed that this strain lost viability quicker than the isogenic homozygous diploid in the S288C background (Figure 5B, 5C; Supplementary Figure 1E). There was a steady rise in red and/or red/white sectored colonies among the survivors during the 37 °C incubation, as expected if the *top2* MC increases genome instability (Figure 5D). We used microarrays to examine genomic alterations in the control FM1873 isolate (no exposure to 37 °C) and in isolates exposed to 37 °C for 6 h, and then allowed to form colonies at 25 °C (Figure 5E; see also Supplementary Information for interpretation on the genomic alterations picked up by SNP array). It is important to stress that the

SNP microarrays allow analysis of genomic alterations throughout the genome in addition to those changes that occur on chromosome V [36, 37]. When the control FM1873 strain was examined before exposure to the restrictive temperature, surprisingly, we found that it was altered relative to an isogenic *TOP2*/*TOP2* hybrid [40]. More specifically, we realized that FM1873 carried a terminal loss of heterozygosity (T-LOH) on the right arm of chromosome XII (the longest chromosome arm in yeast). In addition, all isolates had three to four copies of chromosome XIV. We tried several times to recreate the hybrid *top2-5* diploid but were unable to isolate a derivative that had only two copies of XIV. Since this chromosome is the location of *top2-5*, it is likely that chromosome XIV trisomes and tetrasomes have a selective growth advantage at the permissive temperature over the diploids that have only two *top2-5* copies. We generated an isogenic derivative of FM1873 (MD684) that lacked the T-LOH event on XII, although it still had extra copies of XIV. For our subsequent genomic analyses, we studied both FM1873 and MD684.

The experimental strains were exposed to the restrictive temperature of 37 °C by incubating the cells for six hours either on plates or in liquid (details in Materials and Methods); these two protocols resulted in similar levels of instability. A total of 27 isolates were examined for FM1873 (13 experimental, 14 control), and 19 isolates of MD684 (10 experimental, 9 control). Somewhat surprisingly, the control single-colony isolates (cells not exposed to 37 °C) also had high rates of instability (Table 1; "C" samples), indicating that the Top2p encoded by *top2-5* does not have wild-type activity even at the permissive temperature. Indeed, a previous biochemical study reported that the Top2-5 activity at 25 °C is 33% of that of wild type Top2 [41]. Among all isolates examined, we found 76 T-LOH events, 3 interstitial LOH (I-LOH) events, 31 trisomies, 2 monosomies, and 6 uniparental disomies (UPDs) (Figure 5E; Table 1). The average number of genetic changes per strain (including all the data of Table 1) was 3.3 alterations/isolate. Since the strains were grown approximately 40 generations before microarray

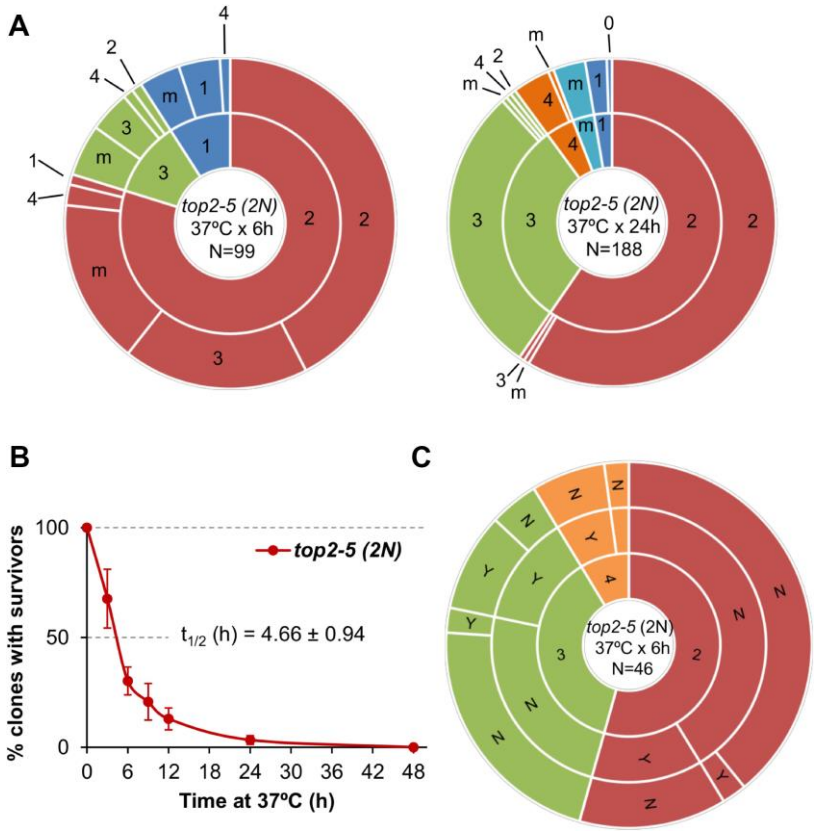

Figure 4. Mitotic catastrophe in *top2-5* diploids leads to progeny with a greater capacity for cell division than observed in the haploid. Isogenic homozygous *top2-5* diploid cells were grown and spread at either low or high cell density on Petri dishes. In addition, G_1/G_0 cells were micromanipulated, arrayed and treated as described in Figure 2C. (**A**) Ability to re-bud after transient (6 h or 24 h) incubations at 37 °C of the high-density plates. The experimental procedure is described in Figure 2. (**B**) Clonogenic survival profile as determined on the low-density plates (mean ± s.e.m., n=3). The experimental procedure is described in Figure 1D. (**C**) Capability of the progeny to split apart and relationship with overall survivability. The experimental procedure is described in Figure 2C.

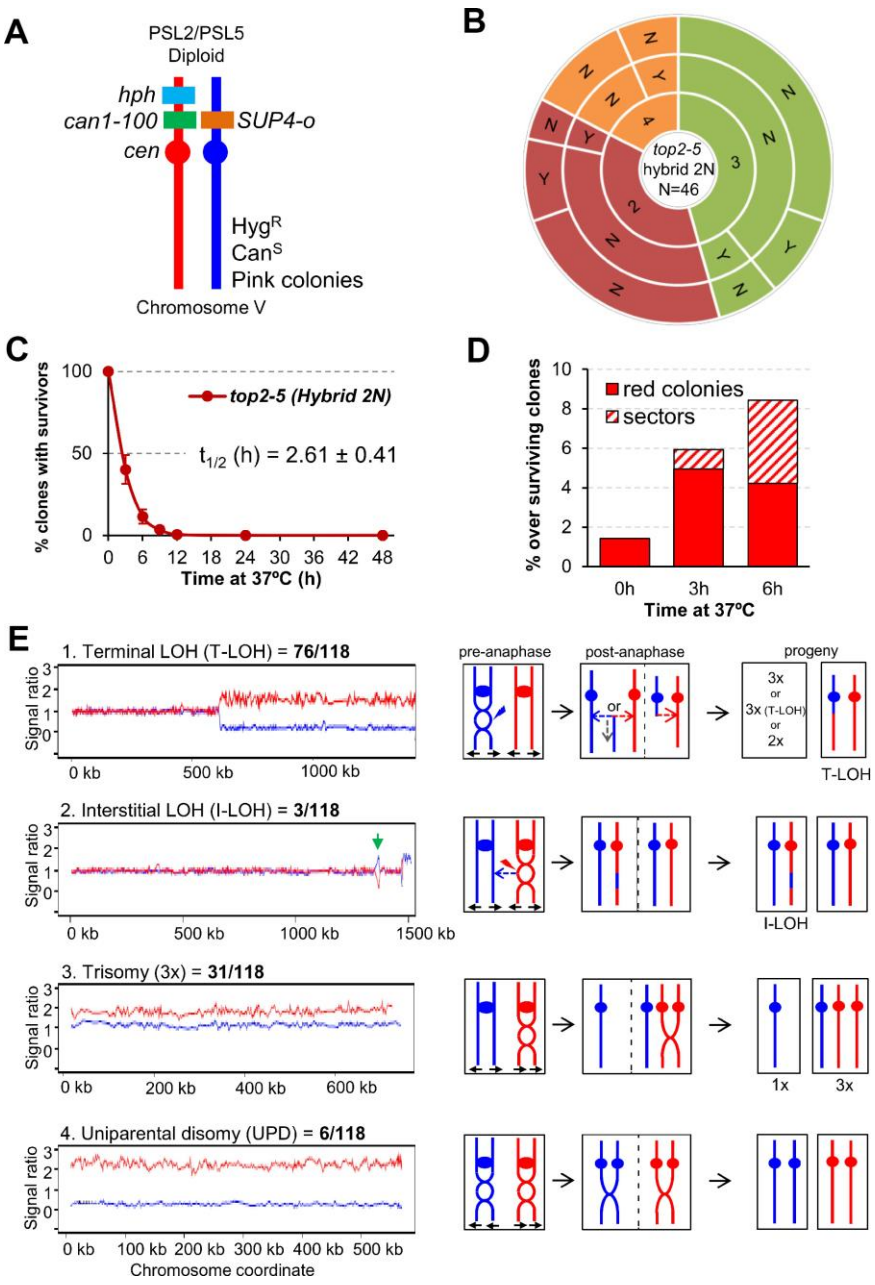

Figure 5. Mitotic catastrophe in *top2-5* heterozygous diploids leads to survivors with specific genetic instability footprints. (**A**) Schematic of the engineered chromosome V (cV) from the hybrid highly heterozygous (~55,000 SNPs) diploids used in this study. As explained in the text, the genetic modifications applied in cV allowed for selection of chromosome rearrangements. (**B**) G_1/G_0 cells from the hybrid highly heterozygous *top2-5* diploid FM1873 strain were micromanipulated, arrayed and treated as described in Figure 2C. The capability of the immediate progeny to split apart and its relationship with overall survivability is shown in the sunburst chart. (**C**) Clonogenic survival profile of FM1873 as determined on low-density plates (mean ± s.e.m., n=3). The experimental procedure is described in Figure 1D. (**D**) Percentage of red or sectored (either white:red or pink:red) colonies in the surviving clones. Both outcomes often reflect genetic alterations on cV as described in the text. (**E**) Results of SNP microarray analysis of colonies derived from FM1873 or MD684. Microarray patterns showing specific chromosome rearrangements are shown on the left side, and diagrams of the putative events producing these patterns are shown on the right side. The number of specific events out of 118 total events is indicated. For the microarray patterns, hybridization to SNPs specific to homologs derived from W303-1A are shown in red, and hybridizations to SNPs specific to YJM789 are shown in blue. The X-axis shows SGD coordinates for the chromosome, and the Y-axis shows the ratio of hybridization normalized to a heterozygous diploid strain. The representative examples correspond to (1) a T-LOH event on chromosome IV (MD684.1.1 (E1) in Table 1); (2) a I-LOH event (marked with a green arrow) plus T-LOH event on chromosome IV (FM1873-15c (C2) in Table 1); (3) a Trisomy for chromosome XIV (MD684.1.1 (E1) in Table 1); and (4) a UPD for chromosome V (This isolate has two copies of the W303-1A-derived and no copies of the YJM789-derived chromosome).

analysis, the rate of alterations/cell division/isolate is about 8.3 x 10^{-2}. In a previous microarray analysis of a wild-type diploid isogenic with FM1873 and MD684, we found a rate of alterations of about 2 x 10^{-3}/division, a rate about 40-fold less than for the *top2* strains. The most common alteration in the *top2* strains was a T-LOH event (64% of the total events). These events likely reflect the repair of a DSB by either a crossover or a break-induced replication (BIR) event (Figure 5E). The chromosomal distribution of the events is striking. The right arms of chromosome IV and XII (the two longest arms in the yeast genome) had over 80% of the terminal LOH events (60/76), although these arms represent less than 30% of the yeast genome. Other chromosomes with T-LOH events (the number of events shown in parentheses) are: XIII (5), XV (4), VII (3), XIV (2), VII (1), XI (1), and V (1). Chromosomes XIII, XV and XIV have the third, fourth, and fifth longest chromosome arms in the genome, respectively; all of the mapped events in these chromosomes are on the longest arms. Strikingly, the very large (about 1.2 Mb) ribosomal RNA gene cluster (rDNA) on the right arm of chromosome XII was not a preferred site for T-LOH events. Although the rDNA is about 60% of the right arm of XII, only 30% (3 of 11) of the LOH events had a breakpoint in or near the rRNA genes. We should point out that T-LOH events on XII could only be followed in the MD684 strains (FM1873 already had a cXIIr T-LOH); hence, our estimate of the frequency of T-LOH events on the right arm of XII is a minimal estimate.

In addition to LOH events, we observed 33 changes in chromosome number (31 trisomies and 2 monosomies) (Table 1). The frequencies of trisomies are not simply related to the size of the chromosomes. Chromosomes V, VIII, and XV were the most frequently-observed trisomes; chromosomes V and VIII are medium-sized chromosomes (both about 550 kb), whereas chromosome XV is large (1092 kb). Only one trisomy was observed involving one of the three smallest chromosomes (I, VI, and III). Only three of the trisomies involved the two largest chromosomes IV and XII.

We also observed six UPD events (Figure 5E). In strains with these events, the homolog is present in two copies, but both copies are derived from one of the original parental homologs. There are two plausible pathways to generate UPD (Supplementary Figure 7): two non-disjunction events in different cell cycles or reciprocal UPD (RUPD) in which one pair of homologs segregates into one cell and the other pair segregates into the other cell. Although both pathways probably contribute to UPD in yeast, at least some of the events in wild-type strains are RUPD [42]. To determine whether RUPD events occurred frequently in the *top2* cells, we used a protocol in which both daughter cells produced as a result of RUPD or a reciprocal crossover (RCO) in chromosome V could be recovered in different sectors of a sectored colony (Supplementary Figure 8). The sectored colonies were derived from the same strains (FM1873 and MD684) used for our single-colony analysis. A crossover or RUPD can produce a red/white sectored colony. However, to select for such events, both FM1873 and MD684 contained a heterozygous *can1-100* marker located allelically to the *SUP4-o* insertion and a gene encoding hygromycin resistance (*hph*) located distal to the *can1-100* insertion (Figure 5A). The *can1-100* mutation is a nonsense mutation and is suppressed by *SUP4-o*. Strains that lack the suppressor are resistant to the drug canavanine and those with the suppressor are sensitive. A crossover between *can1-100* and the centromere results in formation of a canavanine-resistant red/white sectored colony (Supplementary Figure 8A); a sectored colony with the same phenotype can also result from RUPD (Supplementary Figure 8B). RCO and RUPD events can be distinguished by microarray analysis (bottom panels of Supplementary Figure 8).

Following exposure of FM1873 and MD684 to 37 °C, we found 242 red/white Can^R sector colonies, 43 of which had the sectoring pattern for the *hph* marker suggestive of RCO or RUPD events. We found both RCO and RUPD events in two-thirds of these colonies (Supplementary Table 2). The rate of RUPDs in cells of FM1873 and MD684 treated for 6 h at 37 °C was the same, 1.1 x 10^{-5}/division; the rate of RUPD in cells of FM1873 that were not exposed to 37 °C was 1 x 10^{-6}. The rate of RCO in FM1873 cells treated at 37 °C was 2.7 x 10^{-6}; no RCO events were observed in MD684. In an isogenic wild-type strain, the rates of RUPD and RCO for chromosome V were 10^{-7} and 1.6 x 10^{-6}, respectively [42]. These results support the conclusion that the *top2* mutation results in a substantially elevated rate of RUPD (about 100-fold) and has little effect on the rate of RCO.

DISCUSSION

The formation of anaphase chromosome bridges during the cell division is one of the most dramatic sources of genetic instability. Such bridges are expected to cause a MC that would kill most of the progeny. Downregulation of Top2 is likely the most common way of generating large numbers of anaphase bridges. In addition, downregulation of Top2 has important clinical implications during acquisition of resistance against cancer therapy that comprises Top2 poisons (for example, etoposide and anthracyclines). In the present work, we have studied the consequences of inactivating Top2 in yeast through the *top2-5* thermosensitive allele. We show that the expected MC often leads to progeny

Table 1. Genomic changes in single-colony isolates of FM1873 and MD684.

Strain name[1]	Genomic alterations[2]
FM1873-01 (E1)	T-LOH (IV/966), Tri (V), Partial UPD (VII), Tri (X)
FM1873-04 (E1)	T-LOH (IV/471), UPD (VIII), 3 T-LOH (XIII/450/777/864)
FM1873-11 (E1)	UPD (IV), Tri (VIII), Mon (IX), Tri (X), Partial Tri (XV), UPD (XVI)
FM1873-1 (E2)	UPD (IV), Tri (XV)
FM1873-2 (E2)	T-LOH (IV/790)
FM1873-3 (E2)	T-LOH (IV/790)
FM1873-4 (E2)	T-LOH (IV/671), Tri (V), Tri (VII), T-LOH (XV/1002)
FM1873-5 (E2)	T-LOH (IV/755), T-LOH (XIII/450)
FM1873-11X (E2)	T-LOH (IV/958), Tri (VII)
FM1873-12 (E2)	Tri (VIII)
FM1873-13 (E2)	T-LOH (IV/668), Tri (V), T-LOH (XV/1002)
FM1873-14 (E2)	T-LOH (IV/1018)
FM1873-15 (E2)	T-LOH (IV/483)
FM1873-C1 (C1)	No additional alterations
FM1873-C2 (C1)	No additional alterations
FM1873-C3 (C1)	2 T-LOH (IV/485/820)
FM1873-C4 (C1)	T-LOH (IV/470), T-LOH (XIII/856), T-LOH (XIV/216)
FM1873-1c (C2)	2 T-LOH (IV/456/1440); T-LOH (VII/385), T-LOH (XIV/400)
FM1873-2c (C2)	2 T-LOH (IV/957/1440)
FM1873-3c (C2)	T-LOH (IV/935), Tri (V)
FM1873-4c (C2)	T-LOH (IV/858)
FM1873-5c (C2)	Tri and T-LOH (IV/1270), Tri (V), Partial Tri (XIII)
FM1873-11c (C2)	T-LOH (IV/1017), Tri (VIII), Tri (XV)
FM1873-12c (C2)	T-LOH (IV/1004), Tri (X), Tri (XV)
FM1873-13c (C2)	T-LOH (IV/1017), Tri (VIII)
FM1873-14c (C2)	2 T-LOH (IV/889/1221)
FM1873-15c (C2)	I-LOH (IV/1354-1357), T-LOH (IV/1474), Tri (V), UPD (VIII)
MD684.1.1 (E1)	T-LOH (IV/596), T-LOH (XI/7.5), T-LOH (XII/430)
MD684.1.2 (E1)	T-LOH (IV/808), Tri (VIII)
MD684.1.3 (E1)	T-LOH (IV/1002), T-LOH (XII/165)
MD684.1.4 (E1)	T-LOH (IV/458), Tri (XV)
MD684.1.5 (E1)	T-LOH (IV/1065), Tri (VIII), 2 T-LOH (XII/253/446)
MD684.1.6 (E2)	Partial Tri (II)
MD684.1.7 (E2)	T-LOH (IV/1028), T-LOH (VII/29), T-LOH (XII/175)
MD684.1.8 (E2)	3 T-LOH (IV/921/1050/1070), T-LOH (V/538), T-LOH (XII/450)
MD684.1.9 (E2)	Partial Mon (I), Tri and T-LOH (IV/486)
MD684.1.10 (E2)	2 T-LOH (IV/661/963), Tri and T-LOH (XV/626)
MD684 C1.1 (C1)	I-LOH (IV/747-760), T-LOH (IV/840), T-LOH (XII/176)
MD684 C1.2 (C1)	T-LOH (IV/458), T-LOH (XII/447)
MD684 C1.3 (C1)	2 T-LOH (IV/893/1472), Tri (V), T-LOH (XII/170)
MD684 C1.4 (C1)	Tri (I), T-LOH (IV/920)
MD684 C1.5 (C1)	T-LOH (IV/527), Tri (XII)
MD684 C1.6 (C2)	2 T-LOH (IV/680/1050), T-LOH (VII/760), T-LOH (XII/175)
MD684 C1.7 (C2)	T-LOH (IV/1008), I-LOH (XII/215-228), T-LOH (XII/277), Partial Tri (XVI)
MD684 C1.8 (C2)	T-LOH (IV/842), T-LOH (XV/657)
MD684 C1.9 (C2)	T-LOH (IV/1028)

[1] Parentheses after the strain name indicate whether the strain was experimental (E, incubated for six hours at 37 °C) or control (C, not incubated at 37 °C). E1 and C1 indicates that the 37 °C incubation was done on plates; in E2 and C2 experiments, the 37 °C incubations were done in liquid.
[2] Strains derived from FM1873 (both experimental (incubated at 37 °C for six hours) and control (not incubated at 37 °C) strains had three to four copies of chromosome XIV and a terminal LOH event on the right arm of chromosome XII (breakpoint at 236 kb). These alterations, therefore, are not listed in the FM1873 strains. The MD684 strain also had three to four copies of chromosome XIV in isolates, and this alteration is not shown in the table. Code: T-LOH (terminal LOH event), I-LOH (interstitial LOH event), Tri (trisomy), Mon (monosomy), UPD (uniparental disomy). Between brackets: altered chromosomes/breakpoints.

unable to divide; however, cell death is not immediate but the result of a decline in cell vitality that takes hours to complete. We further propose that the irreversible genomic imbalances that occur during chromosome segregation in the absence of Top2 explain the short-term senescence observed in the immediate progeny. This hypothesis is strengthened by the observation that diploid survivors of a *top2* MC often carry genomic footprints expected from anaphase bridges such as UPDs and T-LOH. A step-by-step summary of the *top2* MC events is shown in Figure 6.

We would like to point out there are many different strategies to abolish Top2 activity, from depleting the enzyme through degron systems to using catalytically dead mutants. In between, there are a large collection of conditional thermosensitive alleles. Baxter and Diffley [24] showed that depletion of Top2 had a different phenotype than expression of a catalytically-dead enzyme. Depletion of Top2 did not lead to cell-cycle delays but did result in lethal DNA damage during cytokinesis. In contrast, a mutation in the Top2 catalytic domain resulted in arrest in G_2/M as a consequence of DNA damage (nicks and gaps). The absence of a G_2/M arrest is also a common pattern of thermosensitive alleles [13, 22–26], with the remarkable exception of top2-B44 (F977L), which delays cells in G_2/M through activation of the spindle assembly checkpoint [26]. In addition, we must consider post-G_2/M delays since the NoCut checkpoint slows down cytokinesis under the presence of anaphase bridges [43]. This was shown using the *top2-4* allele, and this delay affects the synchrony of the MC. We previously examined the kinetics of both completion of cytokinesis and severing of anaphase bridges in *top2-4* and *top2-5* [25]. We found that the *top2-5* strain severed the bridge more efficiently and synchronously than *top2-4*, arguing that *top2-5* is a better allele to model *top2* MC; hence, we used this allele to address the *top2* MC. It would be interesting, though, to address the consequences of *top2* MC in other models, including degron-assisted Top2 depletion, partial inactivation (semipermissive conditions) and *top2-ts* alleles that delay either G_2/M or cytokinesis.

On the short-term cytological consequences of the *top2* mitotic catastrophe

In this study we have adopted the term mitotic catastrophe (MC) in its broadest cytological sense, referring to aberrant mitoses that are expected to be deleterious for the progeny based on the degree of observed abnormalities. It is worth mentioning that other authors, especially those working with metazoans, restrict the MC term to death occurring in mitosis after a mitotic insult [44, 45]. With this restriction in mind, MC in metazoans is a sort of mitotic RCD. In our yeast experimental model with the *top2-5* allele, death before anaphase is insignificant since cells go through G_2/M and anaphase as quickly as their *TOP2* counterparts [25]. In nocodazole-treated cells, which arrest cells in G_2/M, 40% cell death was reported after 10 h in clonogenic assays [46]. This cell death was described to occur through an RCD apoptosis-like mechanism. By contrast, our clonogenic assays showed that a sudden drop in viability occurs between 3-6 h after Top2 inactivation (Figure 1D), about the time needed for cells to complete telophase and cytokinesis on solid medium [25]. From the microcolony experiments, we concluded that the ensuing *top2-5* progeny are largely impaired in entering a second cell cycle (Figures 1A, 1B and 2). This impairment can be partly alleviated in diploids, yet only in the short-term (Figure 4). This observation leads us to propose that gross genomic imbalances prevent the immediate progeny from cell cycle progression. Taking into account previous reports on the formation of anaphase bridges in *top2-ts* mutants [13, 25] and high levels of chromosome missegregation [23], it appears logical that many of the haploid progeny lose entire chromosomes containing essential genes. In addition, loss of essential genes may reflect breakage of chromosomes at the bridge followed by loss of the distal chromosome regions [11].

Another possibility is that daughter cells immediately die upon the *top2* MC through an RCD program. This would imply that either anaphase/telophase cells or their immediate progeny sense the MC and execute an RCD. Our results, however, argue against this possibility. Firstly, many cells stained negative for

death (PI) and apoptotic (annexin V) markers, whereas they stained positive for metabolic activity (FUN1©), even after 24 h at 37 °C. Secondly, the decline in cell vitality occurred slowly, linearly (asynchronously) and asymmetrically (when comparing daughter cells that remained together after the MC). Thirdly, Yca1/Mca1, the main RCD player in *S. cerevisiae*, does not regulate the vitality decline. Even though there are other RCD proteins aside from Yca1/Mca1 [47, 48], we point out that that the pattern of cell death after the *top2* MC is better explained through ACD. Although we found intrinsic ROS production in a minor subset of the *top2* MC progeny, and this finding has been considered a marker of RCD [31, 49], we hypothesize that, in our case, ROS accumulation is a consequence of the steady decline of cell homeostasis. For instance, ROS might arise from loss of nuclear genes involved in eliminating ROS in metabolically active cells.

Comparing with previous studies, the events that lead to death after the *top2* MC resemble those observed after prolonged G_2/M arrest in the *cdc13-1* mutant, which results in irreversible DNA damage at chromosome ends. In arrested *cdc13* cells, there are cell markers of RCD such as ROS production [50], although further biochemical assays and genetic manipulation suggest ACD rather than RCD [47]. In *cdc13-1*, because cells get blocked in G_2/M, there are no genetic imbalances prior to cell death. It was proposed that cell lysis, resulting from cell growth without cell division, was the ultimate cause of death, a hypothesis confirmed because sorbitol (an osmotic stabilizer) improved cell viability [47]. Although we also observed oversized cells one day after the *top2* MC (Figure 2A and 2D), cell lysis was a rare event and sorbitol did not improve cell viability (Figure 2D–2F). Therefore, we propose that the secondary ACD observed after the *top2* MC is the consequence of the steady decline of cell homeostasis resulting from loss of essential genes.

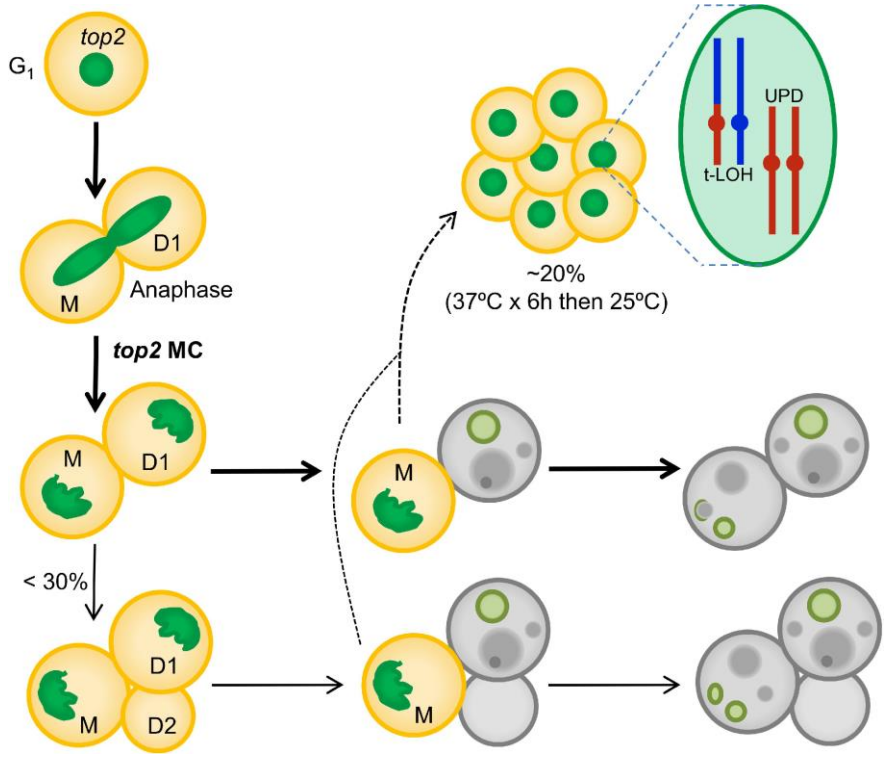

Figure 6. Summary of the *top2*-mediated mitotic catastrophe and the fate of the immediate progeny. After inactivation of Top2, cells cannot resolve sister chromatids in anaphase, leading to an anaphase bridge between the mother (M) and its daughter (D1). These bridges are quickly severed (at least in the *top2-5* mutant [25]). The immediate progeny coming from the *top2* mitotic catastrophes (MCs) is largely unable to enter a new cell cycle (do not re-bud) despite remaining metabolically active for many hours; hence, these cells become senescent. Only ~25% of the original mothers re-bud once (D2) after the *top2* MC. The long-term fate of most daughter cells is death. They will eventually die through accidental cell death (ACD), as deduced from both the asynchrony and asymmetry of death events and the lack of regulation by the death modulator Yca1(Mca1). The inability to enter a new cell cycle is likely a consequence of both the massive DNA damage as a consequence of bridge severing, and the misdistribution of essential genetic material coded on the chromosome arms between the daughter cells. A small proportion of the progeny, especially those cell that underwent a milder *top2* MC (e.g., already in S/G_2 at the time of Top2 inactivation) survives to yield a population of cells with characteristic footprints of genomic instability. Two of these footprints, terminal loss of heterozygosity (T-LOH) and uniparental disomy (UPD) are expected outcomes from anaphase bridges.

On the long-term genetic consequences of the *top2* mitotic catastrophe

We have also compared the genomes of surviving diploids after 6h of Top2 inactivation. Even though we did not prove that all survivors came from a MC (i.e., they went through anaphase), the results shown in Figures 1–5, together with previous findings [13, 24, 25] lead us to conclude that most of these survivors likely came from a *top2* MC. Indeed, many of the observed chromosome variations and rearrangements can be best explained if cells go through anaphase in the absence of proper sister chromatid disjunction [11]. One interpretation of the strong bias for T-LOH events relative to I-LOH events (76 terminal and 3 interstitial) is that DSBs are repaired primarily through BIR (Figure 5E) [11, 51]. In many previous studies, I-LOH represented a very significant fraction of the total LOH events. For example, in G_1-synchronized cells treated with ultraviolet light, we observed a 1:3 ratio between T-LOH and I-LOH [40]. I-LOH requires both ends of the DSB to invade the other homolog during repair through homologous recombination, a condition difficult to fulfil in DSBs generated by cytokinesis [11].

According to a previous study [52], the frequency of DSBs in *top2* mutants is higher for long chromosome arms than short chromosome arms. Spell and Holm [50] explained this observation by suggesting that intertwinings on short chromosome arms could be resolved by passive diffusion off the end, whereas such intertwinings on long chromosome arms required Top2. Our results are also consistent with this interpretation. Chromosome IV and XII right arms are the longest in the yeast genome and are overrepresented in the T-LOH events (normalizing for the size of the arm). An unusual feature of the T-LOH data is the rDNA is under-represented as a breakpoint in the cXIIr T-LOH events. It was previously shown, using an assay that detects loss of inserted marker within the rDNA, that *top2* strains have substantially elevated rates of mitotic recombination in the rDNA [53]. One possible explanation of this discrepancy is that DSBs within the rDNA may be repaired by single-strand annealing between flanking copies of the rDNA genes [54], an event that would result in loss of an inserted marker without an interaction with the other homolog. Such an event could not be detected by the microarray analysis.

Another genetic alteration that is consistent with sister chromatid non-disjunction at the *top2* MC is the elevated presence of trisomies. A straightforward explanation for this is that the intertwining of sister chromatids in the *top2* strains often results in their co-segregation into one of the daughter cells (Figure 5E). Although this type of non-disjunction would be expected to create equal numbers of monosomic and trisomic strains, it is possible that the monosomic strains have a competitive growth disadvantage and are, therefore, selected against. In *tel1 mec1* diploids, expected to enter anaphase with broken and/or underreplicated chromosomes, trisomies were five times more common than monosomies [55]. A similar bias towards trisomies was observed in *cdc14-1* diploids [51]; *cdc14* results in elevated levels of anaphase bridges because Cdc14 regulates condensin and Top2 actions in anaphase [56–58].

Lastly, the 100-fold enrichment in RUPD after the *top2* MC is also in agreement with models of genomic instability generated by sister chromatid non-disjunction. Two models are proposed for the generation of RUPD. One model involves two independent missegregation events occurring in successive divisions. In the other model, segregation of the chromosomes occurs in a manner similar to meiosis-I (Supplementary Figures 7 and 8). In wild-type cells, we demonstrated that the second model is correct [42]. From our data in the current study, we cannot distinguish between these models. The rate of a single non-disjunction event of chromosome V in a *top2* mutant is very high, about 3×10^{-3}/division [23]. Thus, the likelihood of two independent non-disjunction events in a single division is $(3 \times 10^{-3})^2$ or 10^{-5} which is close to our observed rate of RUPD in the *top2-5* diploid. It is possible that both mechanisms contribute to the high rate of RUPD observed in the *top2-5* mutants. Another difference with our earlier study [42] is the low frequency (18%) of sectors reflecting RUPD and RCO recovered from the red/white Can^R sector assay. In our previous study, almost all sectored colonies reflected RCOs or RUPD events. It is likely that the high levels of aneuploidy observed in the *top2* mutants affects colony color by mechanisms unrelated to RCO or RUPD events on chromosome V.

In conclusion, we have characterized the consequences for the progeny of depleting yeast cells of Top2. We determined that the *top2* mitotic catastrophe leads to the sudden loss of the capability to divide again. Nevertheless, restrictions for cell division are not a consequence of immediate cell death as the progeny remain alive for several hours. In addition, survivors of the *top2* mitotic catastrophe carry genomic footprints that point towards sister chromatid non-disjunction and breakage of anaphase bridges as the source of the *top2*-driven genome instability. Overall, the *top2*-mediated mitotic catastrophe is highly deleterious for the cell progeny but it might also bring about highly unstable surviving clones.

MATERIALS AND METHODS

Strain construction

All strains used in this work are listed in Supplementary Table 3. Gene deletions were achieved using standard PCR and transformation methods [25, 59]. To obtain the transformation products, genomic DNA of the corresponding strain in the Euroscarf yeast haploid *MAT*a knockout collection was used as the PCR template. Primers used in the PCR bind 100-400 bps upstream and downstream the deleted gene ORF (Supplementary Table 4).

The *top2-5* isogenic homozygous diploid derivative was generated through a one-step marker-free transformation approach that takes advantage of the α-factor hypersensitivity in the haploid *MAT*a *bar1*Δ genotype (a proof of concept is provided in Supplementary Figure 9). Further details in Supplementary Information.

The *top2-5* heterozygous diploids FM1873 and MD684 were obtained by crossing of haploid strain *top2-5* derivatives of PSL2 and PSL5 (see Supplementary Information). These two strains are isogenic with W303-1A and YJM789, respectively, and have been engineered to select and visually detect chromosome V rearrangements (Figure 5A) [38]. W303-1A and YJM789 differ by about 55,000 SNPs. Thus, these hybrid heterozygous diploids were also used for genome-scale detection of chromosome rearrangements by SNP arrays (see below).

Unless stated otherwise, all strains were grown overnight in air orbital incubators at 25 °C in rich YPD media (1% w/v of yeast extract, 2% w/v peptone and 2% w/v dextrose) before every experiment.

Assays to assess clone survivability and capability of single cells to divide

A modified clonogenic assay performed on agar plates was used to assess survivability of the progeny after the mitotic catastrophe (details in Supplementary Information). The purpose of this assay was to determine if at least one of the resulting cells in the progeny was still able to raise a new cell population, irrespective of how many times the cell has divided and how many cells in the progeny are viable. Half-life values (t ½), the time in which the clone survival drops to 50%, were calculated adjusting the data to a four-parameter model using Graphpad Prism 7.

The time-lapse microcolony analyses were performed with a 40x long-range objective mounted on a Leica LMD6000 direct microscope (details in Supplementary Information). The cell density on the agar plate surface was set to 25 cells per 10,000 μm^2. The cell volume of the original mother cell in all three frames was calculated assuming a perfect sphere and taking the cell diameter for calculations.

The single cell analysis by micromanipulation was performed on YPD plates with a Singer Sporeplay tetrad microdissector (details in Supplementary Information). Just 12 cells were harvested per plate in order to avoid prolonged incubations at 25° C at the beginning of the experiment.

The segregation and morphology of the histone-labelled nucleus (H2A-GFP) was analyzed by wide-field fluorescence videomicroscopy as described before [25]. Further details in Supplementary Information.

Assays to assess cell vitality and cell death

All the colorimetric and fluorometric assays to assess metabolic competence, ROS production, and plasma membrane permeability were carried out in asynchronous logarithmic cultures grown overnight at 25 °C, adjusting the OD_{600} to 0.2 and incubated them for 24 h at 37 °C. Samples were taken at 0, 4 and 24 h and directly observed under the microscope. Fluorescence microscopy was used instead of flow cytometry because strains were already fluorescent for H2A-GFP. ROS were visualized with 10 µg/ml of 2′,7′-dichlorofluorescin diacetate (DCFH-DA; Sigma-Aldrich; D6883); and 3 µg/ml PI (Fluka; #81845) was used to count dead cells. Both dyes were directly mixed with a 200 µl aliquot of the culture and incubated 15 min at 37 °C in the dark. Cell bodies were considered ROS positive when the cytoplasm stained green in the absence of staining for PI. FUN® 1 (Invitrogen; F7030) staining was done washing 200 µl of each sample with water containing 2% D-(+)-glucose and 10 mM Na-HEPES, pH 7.2, resuspending the cells in the same buffer with 10 µM FUN® 1 and incubating 30 min at 37 °C in the dark. For MB (Sigma-Aldrich; M9140) staining, 1 µl of each sample was mixed with 1 µl of a 0.04% w/v MB solution in water onto a microscope slide and directly visualized (bright field). Staining with FITC-labeled annexin V was undertaken in spheroplasts as previously described [32]. Minor modifications to this protocol were employed; namely, we used the TACS Annexin V-FITC Apoptosis Detection Kit (R&Dsystems; 4830-01-K) as well as 60 units/ml of zymolyase (ZymoResearch; E1005) for cell was digestion.

Analysis of genomic rearrangements using microarrays

Two similar protocols were used to expose heterozygous diploids to the *top2*-mediated MC. For both protocols,

cells were grown in YPD to an optical density of 0.5-1. For one set of experiments (marked as E1 in the tables in the text), the cells were struck for single colonies on plates containing solid YPD medium, incubated for 6 hours at 37 ºC, then incubated at room temperature until colonies had formed. For the second protocol, the cells grown at room temperature were harvested by centrifugation, and resuspended in 37 ºC liquid medium, followed by incubation for 6 hours at 37 °C. Following this incubation, they were struck on YPD plates and incubated at room temperature until colonies were formed. For both protocols, the control cells were struck to room temperature YPD plates without incubating them at 37 ºC. In experiments to detect sectored colonies, the YPD medium was replaced with solid omission medium lacking arginine and containing 120 µg/ml canavanine [39].

We detected LOH events, aneuploidy and UPD using SNP-specific microarrays similar to those used by [60]. The details of this procedure can be found in the Supplementary Information and have been described before [36, 37]. In analysis of single-colony isolates, whole-genome arrays were used (Gene Expression Omnibus [GEO] #GPL20144). For analysis of sectored colonies, we used microarrays specific for the right arm of V, and chromosomes I, III, and VIII (GEO #GPL21274).

Abbreviations

MC: mitotic catastrophe; RCD: regulated cell death; ACD: accidental cell death; DSB: DNA double strand break; MB: methylene blue; PI: propidium iodide; ROS: reactive oxygen species; PS: phosphatidylserine; SNP: single nucleotide polymorphism; LOH: loss of heterozygosity; T-LOH: terminal LOH; I-LOH: interstitial LOH; UPD: uniparental disomy; RUPD: reciprocal UPD; rDNA: ribosomal RNA gene cluster.

ACKNOWLEDGMENTS

We thank other members of both labs and Kerry Bloom for fruitful discussions and help. We also thank Jessel Ayra-Plasencia, Nayra Cabrera-Quintero and Annika Lange for technical help in some of the experiments that required micromanipulation and microcolony counting. We thank Yang Sui for help with Supplementary Figures 7 and 8.

CONFLICTS OF INTEREST

The authors declare no conflicts of interests.

FUNDING

The research was supported by the following grant funders: NIH (R35 GM118020) and Army Research Office (SPS #200531) to Thomas D Petes; Agencia Española de Investigación (BFU2015-63902-R and BFU2017-83954-R) to Félix Machín. Cristina Ramos-Pérez was a recipient of a predoctoral fellowship by the Agencia Canaria de Investigación, Innovación y Sociedad de la Información (ACIISI; TESIS20120109). F.M.'s grants and C.R-P.'s fellowship were co-funded by the European Commission's European Regional Development Fund (ERDF).

REFERENCES

1. Hayashi MT, Karlseder J. DNA damage associated with mitosis and cytokinesis failure. Oncogene. 2013; 32:4593–601. https://doi.org/10.1038/onc.2012.615 PMID:23318447

2. Portugal J, Mansilla S, Bataller M. Mechanisms of drug-induced mitotic catastrophe in cancer cells. Curr Pharm Des. 2010; 16:69–78. https://doi.org/10.2174/138161210789941801 PMID:20214619

3. Galluzzi L, Bravo-San Pedro JM, Vitale I, Aaronson SA, Abrams JM, Adam D, Alnemri ES, Altucci L, Andrews D, Annicchiarico-Petruzzelli M, Baehrecke EH, Bazan NG, Bertrand MJ, et al. Essential versus accessory aspects of cell death: recommendations of the NCCD 2015. Cell Death Differ. 2015; 22:58–73. https://doi.org/10.1038/cdd.2014.137 PMID:25236395

4. Chan KS, Koh CG, Li HY. Mitosis-targeted anti-cancer therapies: where they stand. Cell Death Dis. 2012; 3:e411. https://doi.org/10.1038/cddis.2012.148 PMID:23076219

5. Galluzzi L, Vitale I, Vacchelli E, Kroemer G. Cell death signaling and anticancer therapy. Front Oncol. 2011; 1:5. https://doi.org/10.3389/fonc.2011.00005 PMID:22655227

6. Fulda S, Debatin KM. Extrinsic versus intrinsic apoptosis pathways in anticancer chemotherapy. Oncogene. 2006; 25:4798–811. https://doi.org/10.1038/sj.onc.1209608 PMID:16892092

7. Vitale I, Galluzzi L, Castedo M, Kroemer G. Mitotic catastrophe: a mechanism for avoiding genomic instability. Nat Rev Mol Cell Biol. 2011; 12:385–92. https://doi.org/10.1038/nrm3115 PMID:21527953

8. Hoffelder DR, Luo L, Burke NA, Watkins SC, Gollin SM, Saunders WS. Resolution of anaphase bridges in cancer cells. Chromosoma. 2004; 112:389–97. https://doi.org/10.1007/s00412-004-0284-6 PMID:15156327

9. Ganem NJ, Pellman D. Linking abnormal mitosis to the acquisition of DNA damage. J Cell Biol. 2012; 199:871–81. https://doi.org/10.1083/jcb.201210040 PMID:23229895

10. Quevedo O, García-Luis J, Matos-Perdomo E, Aragón L, Machín F. Nondisjunction of a single chromosome leads to breakage and activation of DNA damage checkpoint in G2. PLoS Genet. 2012; 8:e1002509. https://doi.org/10.1371/journal.pgen.1002509 PMID:22363215

11. Machín F, Quevedo O, Ramos-Pérez C, García-Luis J. Cdc14 phosphatase: warning, no delay allowed for chromosome segregation! Curr Genet. 2016; 62:7–13. https://doi.org/10.1007/s00294-015-0502-1 PMID:26116076

12. Uemura T, Tanagida M. Mitotic spindle pulls but fails to separate chromosomes in type II DNA topoisomerase mutants: uncoordinated mitosis. EMBO J. 1986; 5:1003–10. https://doi.org/10.1002/j.1460-2075.1986.tb04315.x PMID:15957215

13. Holm C, Goto T, Wang JC, Botstein D. DNA topoisomerase II is required at the time of mitosis in yeast. Cell. 1985; 41:553–63. https://doi.org/10.1016/S0092-8674(85)80028-3 PMID:2985283

14. Gorbsky GJ. Cell cycle progression and chromosome segregation in mammalian cells cultured in the presence of the topoisomerase II inhibitors ICRF-187 [(+)-1,2-bis(3,5-dioxopiperazinyl-1-yl)propane; ADR-529] and ICRF-159 (Razoxane). Cancer Res. 1994; 54:1042–48. PMID:8313360

15. Damelin M, Bestor TH. The decatenation checkpoint. Br J Cancer. 2007; 96:201–05. https://doi.org/10.1038/sj.bjc.6603537 PMID:17211475

16. Downes CS, Clarke DJ, Mullinger AM, Giménez-Abián JF, Creighton AM, Johnson RT. A topoisomerase II-dependent G2 cycle checkpoint in mammalian cells/. Nature. 1994; 372:467–70. https://doi.org/10.1038/372467a0 PMID:7984241

17. Nakagawa T, Hayashita Y, Maeno K, Masuda A, Sugito N, Osada H, Yanagisawa K, Ebi H, Shimokata K, Takahashi T. Identification of decatenation G2 checkpoint impairment independently of DNA damage G2 checkpoint in human lung cancer cell lines. Cancer Res. 2004; 64:4826–32. https://doi.org/10.1158/0008-5472.CAN-04-0871 PMID:15256452

18. Brooks K, Chia KM, Spoerri L, Mukhopadhyay P, Wigan M, Stark M, Pavey S, Gabrielli B. Defective decatenation checkpoint function is a common feature of melanoma. J Invest Dermatol. 2014; 134:150–58. https://doi.org/10.1038/jid.2013.264 PMID:23842115

19. Jain CK, Roychoudhury S, Majumder HK. Selective killing of G2 decatenation checkpoint defective colon cancer cells by catalytic topoisomerase II inhibitor. Biochim Biophys Acta. 2015; 1853:1195–204. https://doi.org/10.1016/j.bbamcr.2015.02.021 PMID:25746763

20. Nitiss JL. Targeting DNA topoisomerase II in cancer chemotherapy. Nat Rev Cancer. 2009; 9:338–50. https://doi.org/10.1038/nrc2607 PMID:19377506

21. Holohan C, Van Schaeybroeck S, Longley DB, Johnston PG. Cancer drug resistance: an evolving paradigm. Nat Rev Cancer. 2013; 13:714–26. https://doi.org/10.1038/nrc3599 PMID:24060863

22. DiNardo S, Voelkel K, Sternglanz R. DNA topoisomerase II mutant of Saccharomyces cerevisiae: topoisomerase II is required for segregation of daughter molecules at the termination of DNA replication. Proc Natl Acad Sci USA. 1984; 81:2616–20. https://doi.org/10.1073/pnas.81.9.2616 PMID:6326134

23. Holm C, Stearns T, Botstein D. DNA topoisomerase II must act at mitosis to prevent nondisjunction and chromosome breakage. Mol Cell Biol. 1989; 9:159–68. https://doi.org/10.1128/MCB.9.1.159 PMID:2538717

24. Baxter J, Diffley JF. Topoisomerase II inactivation prevents the completion of DNA replication in budding yeast. Mol Cell. 2008; 30:790–802. https://doi.org/10.1016/j.molcel.2008.04.019 PMID:18570880

25. Ramos-Pérez C, Ayra-Plasencia J, Matos-Perdomo E, Lisby M, Brown GW, Machín F. Genome-Scale Genetic Interactions and Cell Imaging Confirm Cytokinesis as Deleterious to Transient Topoisomerase II Deficiency in *Saccharomyces cerevisiae.* G3 (Bethesda). 2017; 7:3379–91. https://doi.org/10.1534/g3.117.300104 PMID:28839115

26. Andrews CA, Vas AC, Meier B, Giménez-Abián JF, Díaz-Martínez LA, Green J, Erickson SL, Vanderwaal KE, Hsu WS, Clarke DJ. A mitotic topoisomerase II checkpoint in budding yeast is required for genome stability but acts independently of Pds1/securin. Genes Dev. 2006; 20:1162–74. https://doi.org/10.1101/gad.1367206 PMID:16651657

27. Carmona-Gutierrez D, Bauer MA, Zimmermann A, Aguilera A, Austriaco N, Ayscough K, Balzan R, Bar-Nun S, Barrientos A, Belenky P, Blondel M, Braun RJ,

Breitenbach M, et al. Guidelines and recommendations on yeast cell death nomenclature. Microb Cell. 2018; 5:4–31. https://doi.org/10.15698/mic2018.01.607 PMID:29354647

28. Klein HL, Bačinskaja G, Che J, Cheblal A, Elango R, Epshtein A, Fitzgerald DM, Gómez-González B, Khan SR, Kumar S, Leland BA, Marie L, Mei Q, et al. Guidelines for DNA recombination and repair studies: cellular assays of DNA repair pathways. Microb Cell. 2019; 6:1–64. https://doi.org/10.15698/mic2019.01.664 PMID:30652105

29. Kucsera J, Yarita K, Takeo K. Simple detection method for distinguishing dead and living yeast colonies. J Microbiol Methods. 2000; 41:19–21. https://doi.org/10.1016/S0167-7012(00)00136-6 PMID:10856773

30. Millard PJ, Roth BL, Thi HP, Yue ST, Haugland RP. Development of the FUN-1 family of fluorescent probes for vacuole labeling and viability testing of yeasts. Appl Environ Microbiol. 1997; 63:2897–905. PMID:9212436

31. Madeo F, Fröhlich E, Ligr M, Grey M, Sigrist SJ, Wolf DH, Fröhlich KU. Oxygen stress: a regulator of apoptosis in yeast. J Cell Biol. 1999; 145:757–67. https://doi.org/10.1083/jcb.145.4.757 PMID:10330404

32. Madeo F, Fröhlich E, Fröhlich KU. A yeast mutant showing diagnostic markers of early and late apoptosis. J Cell Biol. 1997; 139:729–34. https://doi.org/10.1083/jcb.139.3.729 PMID:9348289

33. Carmona-Gutierrez D, Eisenberg T, Büttner S, Meisinger C, Kroemer G, Madeo F. Apoptosis in yeast: triggers, pathways, subroutines. Cell Death Differ. 2010; 17:763–73. https://doi.org/10.1038/cdd.2009.219 PMID:20075938

34. Madeo F, Herker E, Maldener C, Wissing S, Lächelt S, Herlan M, Fehr M, Lauber K, Sigrist SJ, Wesselborg S, Fröhlich KU. A caspase-related protease regulates apoptosis in yeast. Mol Cell. 2002; 9:911–17. https://doi.org/10.1016/S1097-2765(02)00501-4 PMID:11983181

35. Mitsui K, Nakagawa D, Nakamura M, Okamoto T, Tsurugi K. Valproic acid induces apoptosis dependent of Yca1p at concentrations that mildly affect the proliferation of yeast. FEBS Lett. 2005; 579:723–27. https://doi.org/10.1016/j.febslet.2004.12.051 PMID:15670835

36. St Charles J, Hazkani-Covo E, Yin Y, Andersen SL, Dietrich FS, Greenwell PW, Malc E, Mieczkowski P, Petes TD. High-resolution genome-wide analysis of irradiated (UV and γ-rays) diploid yeast cells reveals a high frequency of genomic loss of heterozygosity (LOH) events. Genetics. 2012; 190:1267–84. https://doi.org/10.1534/genetics.111.137927 PMID:22267500

37. St Charles J, Petes TD. High-resolution mapping of spontaneous mitotic recombination hotspots on the 1.1 Mb arm of yeast chromosome IV. PLoS Genet. 2013; 9:e1003434. https://doi.org/10.1371/journal.pgen.1003434 PMID:23593029

38. Lee PS, Greenwell PW, Dominska M, Gawel M, Hamilton M, Petes TD. A fine-structure map of spontaneous mitotic crossovers in the yeast Saccharomyces cerevisiae. PLoS Genet. 2009; 5:e1000410. https://doi.org/10.1371/journal.pgen.1000410 PMID:19282969

39. Barbera MA, Petes TD. Selection and analysis of spontaneous reciprocal mitotic cross-overs in Saccharomyces cerevisiae. Proc Natl Acad Sci USA. 2006; 103:12819–24. https://doi.org/10.1073/pnas.0605778103 PMID:16908833

40. Yin Y, Petes TD. Genome-wide high-resolution mapping of UV-induced mitotic recombination events in Saccharomyces cerevisiae. PLoS Genet. 2013; 9:e1003894. https://doi.org/10.1371/journal.pgen.1003894 PMID:24204306

41. Jannatipour M, Liu YX, Nitiss JL. The top2-5 mutant of yeast topoisomerase II encodes an enzyme resistant to etoposide and amsacrine. J Biol Chem. 1993; 268:18586–92. PMID:8395511

42. Andersen SL, Petes TD. Reciprocal uniparental disomy in yeast. Proc Natl Acad Sci USA. 2012; 109:9947–52. https://doi.org/10.1073/pnas.1207736109 PMID:22665764

43. Mendoza M, Norden C, Durrer K, Rauter H, Uhlmann F, Barral Y. A mechanism for chromosome segregation sensing by the NoCut checkpoint. Nat Cell Biol. 2009; 11:477–83. https://doi.org/10.1038/ncb1855 PMID:19270692

44. Galluzzi L, Vitale I, Abrams JM, Alnemri ES, Baehrecke EH, Blagosklonny MV, Dawson TM, Dawson VL, El-Deiry WS, Fulda S, Gottlieb E, Green DR, Hengartner MO, et al. Molecular definitions of cell death subroutines: recommendations of the Nomenclature Committee on Cell Death 2012. Cell Death Differ. 2012; 19:107–20. https://doi.org/10.1038/cdd.2011.96 PMID:21760595

45. Burgess A, Rasouli M, Rogers S. Stressing mitosis to death. Front Oncol. 2014; 4:140. https://doi.org/10.3389/fonc.2014.00140 PMID:24926440

46. Endo K, Mizuguchi M, Harata A, Itoh G, Tanaka K. Nocodazole induces mitotic cell death with apoptotic-like features in Saccharomyces cerevisiae. FEBS Lett. 2010; 584:2387–92. https://doi.org/10.1016/j.febslet.2010.04.029 PMID:20399776

47. Wysocki R, Kron SJ. Yeast cell death during DNA damage arrest is independent of caspase or reactive oxygen species. J Cell Biol. 2004; 166:311–16. https://doi.org/10.1083/jcb.200405016 PMID:15289493

48. Váchová L, Palková Z. Caspases in yeast apoptosis-like death: facts and artefacts. FEMS Yeast Res. 2007; 7:12–21. https://doi.org/10.1111/j.1567-1364.2006.00137.x PMID:17311581

49. Perrone GG, Tan SX, Dawes IW. Reactive oxygen species and yeast apoptosis. Biochim Biophys Acta. 2008; 1783:1354–68. https://doi.org/10.1016/j.bbamcr.2008.01.023 PMID:18298957

50. Qi H, Li TK, Kuo D, Nur-E-Kamal A, Liu LF. Inactivation of Cdc13p triggers MEC1-dependent apoptotic signals in yeast. J Biol Chem. 2003; 278:15136–41. https://doi.org/10.1074/jbc.M212808200 PMID:12569108

51. Quevedo O, Ramos-Pérez C, Petes TD, Machín F. The Transient Inactivation of the Master Cell Cycle Phosphatase Cdc14 Causes Genomic Instability in Diploid Cells of Saccharomyces cerevisiae. Genetics. 2015; 200:755–69. https://doi.org/10.1534/genetics.115.177626 PMID:25971663

52. Spell RM, Holm C. Nature and distribution of chromosomal intertwinings in Saccharomyces cerevisiae. Mol Cell Biol. 1994; 14:1465–76. https://doi.org/10.1128/MCB.14.2.1465 PMID:8289822

53. Christman MF, Dietrich FS, Fink GR. Mitotic recombination in the rDNA of S. cerevisiae is suppressed by the combined action of DNA topoisomerases I and II. Cell. 1988; 55:413–25. https://doi.org/10.1016/0092-8674(88)90027-X PMID:2902925

54. Ozenberger BA, Roeder GS. A unique pathway of double-strand break repair operates in tandemly repeated genes. Mol Cell Biol. 1991; 11:1222–31. https://doi.org/10.1128/MCB.11.3.1222 PMID:1996088

55. McCulley JL, Petes TD. Chromosome rearrangements and aneuploidy in yeast strains lacking both Tel1p and Mec1p reflect deficiencies in two different mechanisms. Proc Natl Acad Sci USA. 2010; 107:11465–70. https://doi.org/10.1073/pnas.1006281107 PMID:20534547

56. D'Amours D, Stegmeier F, Amon A. Cdc14 and condensin control the dissolution of cohesin-independent chromosome linkages at repeated DNA. Cell. 2004; 117:455–69. https://doi.org/10.1016/S0092-8674(04)00413-1 PMID:15137939

57. Sullivan M, Higuchi T, Katis VL, Uhlmann F. Cdc14 phosphatase induces rDNA condensation and resolves cohesin-independent cohesion during budding yeast anaphase. Cell. 2004; 117:471–82. https://doi.org/10.1016/S0092-8674(04)00415-5 PMID:15137940

58. Machín F, Torres-Rosell J, Jarmuz A, Aragón L. Spindle-independent condensation-mediated segregation of yeast ribosomal DNA in late anaphase. J Cell Biol. 2005; 168:209–19. https://doi.org/10.1083/jcb.200408087 PMID:15657393

59. Smith JS, Burke DJ. Yeast Genetics: Methods and Protocols. Smith JS, Burke DJ, editors. New York, NY: Springer New York; 2014; 1–375 p. https://doi.org/10.1007/978-1-4939-1363-3

60. Gresham D, Curry B, Ward A, Gordon DB, Brizuela L, Kruglyak L, Botstein D. Optimized detection of sequence variation in heterozygous genomes using DNA microarrays with isothermal-melting probes. Proc Natl Acad Sci USA. 2010; 107:1482–87. https://doi.org/10.1073/pnas.0913883107 PMID:20080586

SUPPLEMENTARY MATERIALS

Interpretation of microcolony assays

Cells from asynchronous cultures were seeded on the surface of a plate at a cell density that optimized distance between cells and number of cells per field. Selected fields normally contain budded ($S/G_2/M$) and unbudded (G_0/G_1) cells, oscillating from a 1:1 to a 1:2 ratio. In our analyses, we concentrated on unbudded cells. A picture was taken before shifting the incubation temperature to 37 ºC (0h), then another picture of the same field was taken after the 37 ºC incubation (either 6h or 24h), and a final third picture was taken the day after, once the plate had been re-incubated at 25 ºC. The situation of each G_0/G_1 cell at the beginning of the assay was monitored after the 37 ºC incubations (6h or 24h) and after the plates were shifted back to 25 ºC. The landscape of possible outcomes is as shown in the Supplementary Table 5 (indicating "cell bodies" that may raise from the one-bodied G_0/G_1 cell). Each G_1/G_0 cells could travel through any of the indicated categories. In the main text, we sometimes refer to their trajectory as, for example, 2 → 1. This indicates that one G_1/G_0 at 0h became 2 bodies after the 37 ºC incubation, but then one body lysed, and the other did not bud again despite reactivating Top2 (25 ºC). Likewise, 3 → m means that the G_1/G_0 cell became a triplet at 37 ºC and then formed a large microcolony after Top2 re-activation. Because the quantification of all trajectories is complex, as shown in the outcome landscape table, we opted for sunburst charts (Figures 2B, 2F, 3E, 4A). The inner circle in the sunburst chart depicts proportions of cell bodies after the 37 ºC incubation. The outer circle depicts proportion of cell bodies after the final 25 ºC incubations for each situation observed in the inner circle. In order to aid with the interpretation of trajectories, we used different colors for different cell body numbers in the inner circle, but kept the colors of the inner circle for the same progeny in the outer circle. The changes in body numbers between the inner and the outer circles are indicated by numbers.

Interpretation of SNP arrays to detect genome rearrangements

Each SNP array contains 25-base oligonucleotides that matched either the W303-1A-associated allele or the YJM789-associated allele for about 13,000 different SNPs (out of 55,000 SNPs). The selected SNPs are distributed evenly across the genome, giving an array resolution of ~1 Kb (yeast genome is 13 Mb, excluding the 1-2 Mb of the repetitive ribosomal DNA array). By measuring the relative amounts of hybridization to each oligonucleotide, we could detect loss of heterozygosity (LOH) (an event expected from mitotic recombination), as well as analyse deletions, duplications, and changes in chromosome number. Examples of these types of genome rearrangements are given in the plots shown in Figure 5E and Supplementary Figure 8. The Y-axis shows the normalized hybridization ratio to probes specific to the W303-1A form of the SNP (red) or the YJM789 form of the SNP (blue). Heterozygous SNPs have ratios of about 1; in LOH events, SNPs derived from one homolog have a ratio of near 2 and those derived from the other have a ratio near 0. One common pattern is a terminal LOH (T-LOH) event, which can reflect either a reciprocal crossover or a non-reciprocal type of recombination termed "break-induced replication" (BIR, Figure 5E) [1]. A second type of LOH is an interstitial LOH event (I-LOH) in which a region of LOH is flanked by heterozygous. I-LOH events (gene conversions) result from the non-reciprocal transfer of DNA sequences between homologs. Two other classes of genomic rearrangements are a consequence of chromosome non-disjunction. Such non-disjunction events can result in trisomy or monosomy. An event in which one homolog is duplicated and another deleted is called "uniparental disomy" (UPD) and can reflect a non-disjunction event in which the two homologs segregate into different daughter cells.

MATERIALS AND METHODS

Construction of the *top2-5/top2-5* isogenic homozygous diploid (FM1730)

We employed the one-step marker-free transformation-based protocol described in Supplementary Figure 9. Briefly, the haploid *MAT*a *bar1*Δ *top2-5 HTA2-GFP* strain used in most experiments (FM1386) was transformed with a PCR product obtained from a *MAT***α** haploid strain. This product is designed such that it can only recombine with the *MAT* locus but not with the silent *HML/HMR* loci. We counterselected against the *MAT*a genotype by spreading 5 µg α-factor on the Petri dish surface before spreading the transformed cells. Colonies resistant to α-factor were collected after 3-4 days at 25 ºC and checked by PCR for the *MAT*a, *MAT*α or *MAT*a/*MAT*α genotypes (Supplementary Figure 9). *MAT*a/*MAT*α diploids were further confirmed by sporulation capability and 2N DNA content by flow cytometry [2].

Construction of the *top2-5/top2-5* hybrid heterozygous diploids (FM1873 and MD684)

The *top2-5* heterozygous diploids FM1873 and MD684 were obtained by crossing of haploid strain

top2-5 derivatives of PSL2 and PSL5. These two strains are isogenic with W303-1A and YJM789, respectively, and have been engineered to select and visually detect chromosome V rearrangements [3]. W303-1A and YJM789 differ by about 55,000 SNPs. The PSL2 *top2-5* (FM1830) and PSL5 *top2-5* (FM1832) haploids were constructed by transformation with a *top2-5:9xmyc:natNT2* product. This product was amplified by PCR from a CH326 strain derivative in which the *top2-5* allele had been tagged at 3' with sequences for 9 copies of the Myc epitope [4]. The heterozygous *top2-5/top2-5* diploid FM1873 was obtained by crossing FM1830 and FM1832. After realizing that FM1873 already carried genome alterations at 25 ºC (3-4 copies of cXIV and cXIIr T-LOH), other attempts to construct this diploid were undertaken. Previously, the FM1830 and FM1832 haploids were analysed and it was determined that FM1830 had 1-2 copies of cXIV. Thus, FM1830 was backcrossed with W303 to cure the strain of genome alterations. One spore (MD681) was identified that had the same genotype as FM1830 except that it had only one copy of chromosome XIV. This strain was crossed to FM1832 to generate the diploid MD684. Although these steps of construction were designed to generate a diploid that was isogenic with FM1873 lacking the aneuploidy of XIV and the T-LOH event on cXIIr, subsequent microarray analysis showed that MD684 still had three to four copies of XIV, although the T-LOH event on cXIIr was absent.

Clonogenic survivability assays

Clonogenic assays were performed directly on agar plates to determine survivability of the progeny regardless the actual number of daughter cells originated at the restrictive condition. For this purpose, 10^2 and 10^3 cells (as estimated after counting cells in an asynchronous logarithmic culture with a Neubauer chamber) were spread onto a set of 14 YPD plates. These plates were then incubated for 0, 3, 6, 9, 12, 24 and 48 h at 37 ºC. After that, they were switched to 25 ºC to allow the growth of the survivors. Colonies were counted after 3–4 days and were normalized to the number of colonies grown without exposure to the restrictive temperature (0 h).

Microcolony assays

For the microcolony analysis, ~1.5 × 10^5 cells (counted by a Neubauer chamber) were spread onto a YPD (or YPD plus 1.2 M Sorbitol) plate to yield a density on the plate surface of around 25 cells per 10,000 µm^2. Defined positions on the plate were marked by piercing the surface with the needle of a Singer Sporeplay tetrad microdissector, using its 8 × 8 grid as a reference (12-16 fields in total). The plate was then transferred to a Leica LMD6000 direct microscope equipped with a 6.7x and 40x long-range objectives. The 6.7x was used to locate the marked fields and the 40x to take pictures of the cells in those fields (corresponding to 0 h, 25 ºC). Next, the plates were incubated at 37 ºC for 6 or 24 h before taking new pictures of the same fields. The procedure was repeated one more time after incubating the plate back at 25 ºC for 18–24 h. Finally, the same microcolonies in the corresponding three frames per field were identified by eye and categorized as indicated in the figure legends.

Single cell analysis of the progeny by micromanipulation

For micromanipulation of the progeny the different strains were streaked on YPD Petri dishes. Unbudded cells were harvested with a Singer Sporeplay tetrad microdissector. Just 12 cells were harvested per plate and arrayed along the A file stage grid template in order to avoid prolonged incubations at 25º C. They were then incubated 6 h at 37 ºC and then observed under the microscope to count the number of cells that originated from the initial cell. Next, each cell that had at least a new bud was subjected to a mild attempt to separate the cell bodies using the needle and the vibration device. If successful, the largest body remained in the A file, whereas the other body was transferred to the B file. Finally, the plate was incubated 4 d at 25 ºC to search for survivors.

Assays to determine segregation and morphology of the nucleus

The segregation and morphology of the histone-labelled nucleus (H2A-GFP) was analyzed by wide-field fluorescence videomicroscopy. An asynchronous culture was concentrated by centrifugation to OD_{660} of 3 and spread onto YPD agar 90 mm Petri dishes. Patches were made from this plate and mounted on a microscope slide. They were incubated at 37 ºC for 24 h in high humidity chambers to avoid the patch to dry. The same fields were photomicrographed at 0, 6 and 24 h, or as reported before [5]. For each time point, a series of z-focal plane images (10 planes, 0.6 µm depth) were collected on a Leica DMI6000, using a 63x/1.30 immersion objective and an ultrasensitive DFC 350 digital camera, and processed with the AF6000 software (Leica).

SNP microarrays

In brief, for most experiments, genomic DNA was obtained from single-colony isolates of experimental

samples (incubated for six hours at 37 ºC) that was labeled with Cy5-dUTP. Two different types of microarray-control DNA were used and labelled with Cy3-dUTP. For some experiments, we used DNA purified from the FM1873 culture before exposure to 37 ºC. In other experiments, we used DNA from the *TOP2/TOP2* isogenic strain JSC24 [1]. Following labeling of the samples, the experimental and microarray-control DNA samples were mixed and hybridized to the microarrays [6]. The microarrays were then scanned at wavelengths 532 and 635 nm with a GenePix scanner, and analyzed by GenePix Pro software. Hybridization signals for Cy5 and Cy3 were normalized over the array to a value of 1. Additional steps of normalization are described in [6]. Following normalization, the ratio of hybridization of the experimental samples to the control samples for individual SNPs was 1 if the experimental strain was heterozygous.

REFERENCES

1. Yin Y, Petes TD. Genome-Wide High-Resolution Mapping of UV-Induced Mitotic Recombination Events in Saccharomyces cerevisiae. PLoS Genet. 2013; 9. https://doi.org/10.1371/journal.pgen.1003894 PMID:24204306

2. García-Luis J, Machín F. Mus81-Mms4 and Yen1 resolve a novel anaphase bridge formed by noncanonical Holliday junctions. Nat Commun. 2014; 5: 5652. https://doi.org/10.1038/ncomms6652 PMID:25466415

3. Lee PS, Greenwell PW, Dominska M, Gawel M, Hamilton M, Petes TD. A fine-structure map of spontaneous mitotic crossovers in the yeast Saccharomyces cerevisiae. PLoS Genet. 2009; 5: e1000410. https://doi.org/10.1371/journal.pgen.1000410 PMID:19282969

4. Janke C, Magiera MM, Rathfelder N, Taxis C, Reber S, Maekawa H, Moreno-Borchart A, Doenges G, Schwob E, Schiebel E, Knop M. A versatile toolbox for PCR-based tagging of yeast genes: new fluorescent proteins, more markers and promoter substitution cassettes. Yeast. 2004; 21:947–62. https://doi.org/10.1002/yea.1142 PMID:15334558

5. Ramos-Pérez C, Ayra-Plasencia J, Matos-Perdomo E, Lisby M, Brown GW, Machín F. Genome-Scale Genetic Interactions and Cell Imaging Confirm Cytokinesis as Deleterious to Transient Topoisomerase II Deficiency in Saccharomyces cerevisiae. G3 (Bethesda). 2017; 7:3379–91. https://doi.org/10.1534/g3.117.300104 PMID:28839115

6. St. Charles J, Hazkani-Covo E, Yin Y, Andersen SL, Dietrich FS, Greenwell PW, Malc E, Mieczkowski P, Petes TD. High-resolution genome-wide analysis of irradiated (UV and γ-Rays) diploid yeast cells reveals a high frequency of genomic loss of heterozygosity (LOH) events. Genetics. 2012; 190:1267–84. https://doi.org/10.1534/genetics.111.137927 PMID:22267500

7. Haber JE. Mating-type gene switching in Saccharomyces cerevisiae. Annu Rev Genet. 1998; 32:561–99. https://doi.org/10.1146/annurev.genet.32.1.561 PMID:9928492

8. Holm C, Goto T, Wang JC, Botstein D. DNA topoisomerase II is required at the time of mitosis in yeast. Cell. 1985; 41:553–63. https://doi.org/10.1016/S0092-8674(85)80028-3

Supplementary Figures

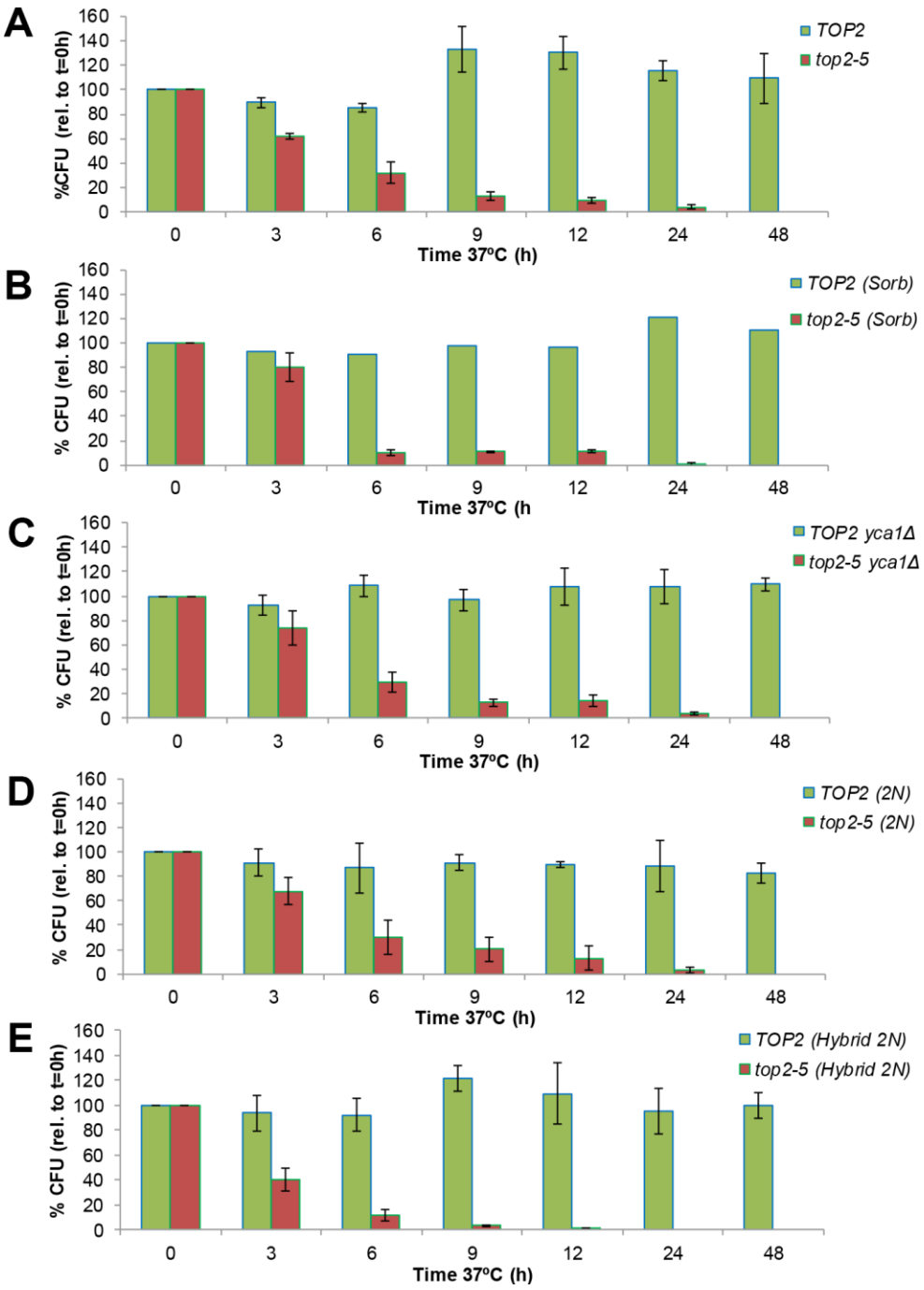

Supplementary Figure 1. Time course of clonogenic survivability of all *top2-5* strains and conditions studied and comparisons with their *TOP2* counterparts. Asynchronous cultures growing at 25 ºC were spread onto several plates for each strain or condition (mean +/- sem, n=3; except for TOP2 strain in Sorbitol where n=1). The plates were incubated at 37 ºC for different periods before transferring them 25 ºC. Four days after the initial plating, visible colonies (macrocolonies) were counted and normalized to a control plate which was never incubated at 37 ºC (0h). (**A**) haploid *top2-5* (FM1386) vs haploid *TOP2* (FM1419) on YPD. (**B**) The same two strains on YPD plus 1.2 M Sorbitol. (**C**) haploid *top2-5 yca1*Δ (FM1856) vs haploid *TOP2 yca1*Δ (FM1871) on YPD. (**D**) Homozygous diploid *top2-5* (FM1730) vs homozygous diploid *TOP2* (FM1732) on YPD. (**E**) Hybrid heterozygous diploid *top2-5* (FM1873) vs hybrid heterozygous diploid *TOP2* (FM2010) on YPD. These charts are related to Figures 1D, 2E, 3D, 4B and 5C, respectively.

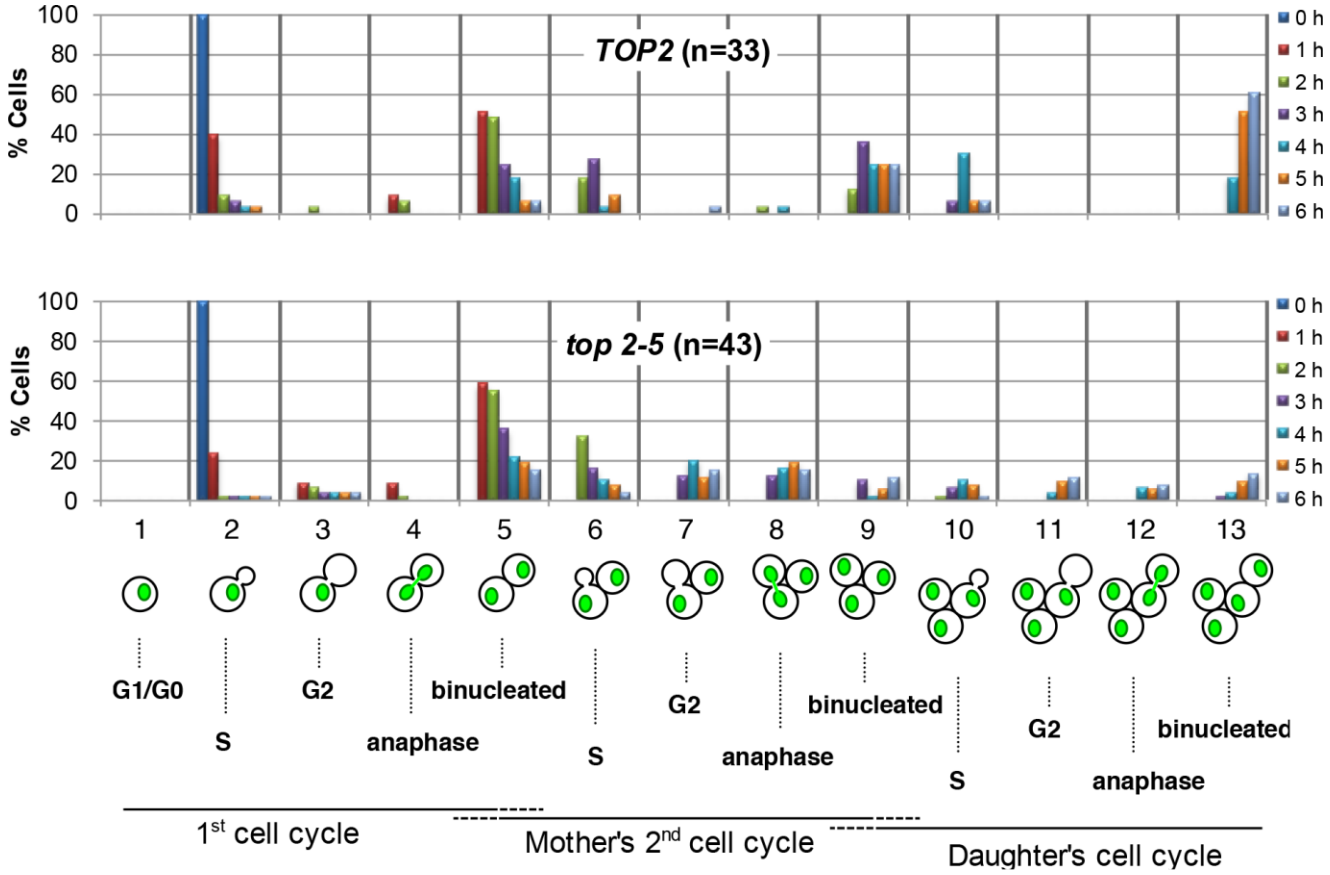

Supplementary Figure 2. Progression of cell division in budded *top2-5* cells at the time of the 37 °C upshift. HTA2-GFP cells carrying either the *TOP2* or the *top2-5* alleles were grown at 25 °C concentrated to OD_{600}=3, spread onto YPD agarose patches and filmed under the microscope in a 37 °C incubation. Total number of cells analysed (N) is indicated for each chart. Each hour, during a period of 6 h, a new photo was taken and each cell was moved to one of the indicated categories depending on whether it has budded, re-budded, segregated or attempted to split the nuclear mass, and whether any of these events have occurred in the mother or the daughter cell coming from the first division. The cells analysed in this experiment come from the same fields in which only unbudded cells at 0 h were followed in the Figure 2A in [5]. In this case, only budded cells at 0 h were considered.

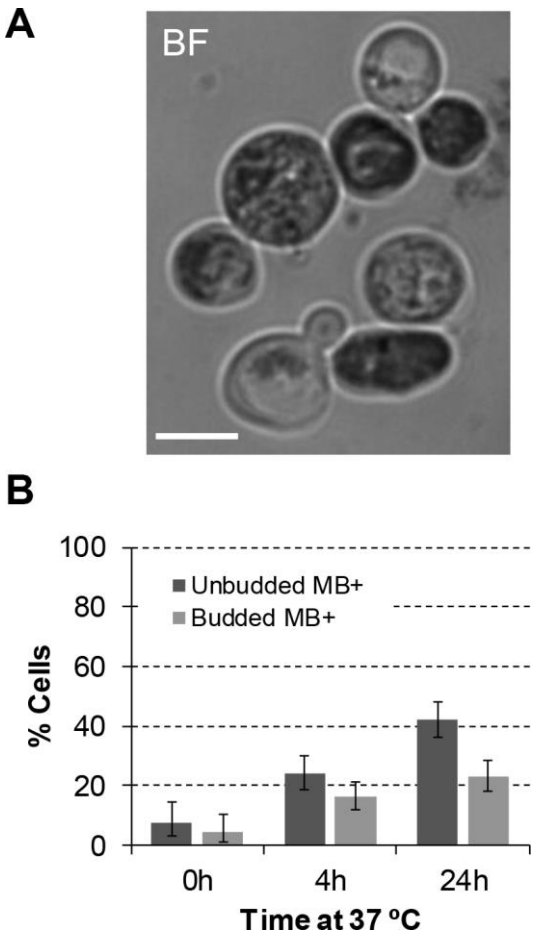

Supplementary Figure 3. Distribution of methylene blue staining in the *top2-5* population after incubation at 37 ºC for 24 h. Related to Figure 3B. (**A**) Examples of cells that stained or not blue (dark grey in the image) after 24 h at 37º C. Note at the bottom of the image a triplet (mother with two attached daughters) where only one cell body (first daughter) has lost vitality. Scale bar depicts 5 µm; BF, bright field. (**B**) Percentage of MB+ cells at 0, 4 and 24 h at 37 ºC (± CI95). Cells were firstly classified as unbudded or budded (2-3 cell bodies). Budded cells were scored as MB+ if at least one body stained positive. The unbudded:budded ratio was ~2:1 in this experiment. Thus, the 40%:20% ratio after 24 h at 37 ºC implies that unbudded and budded cells are equally stained in relative terms.

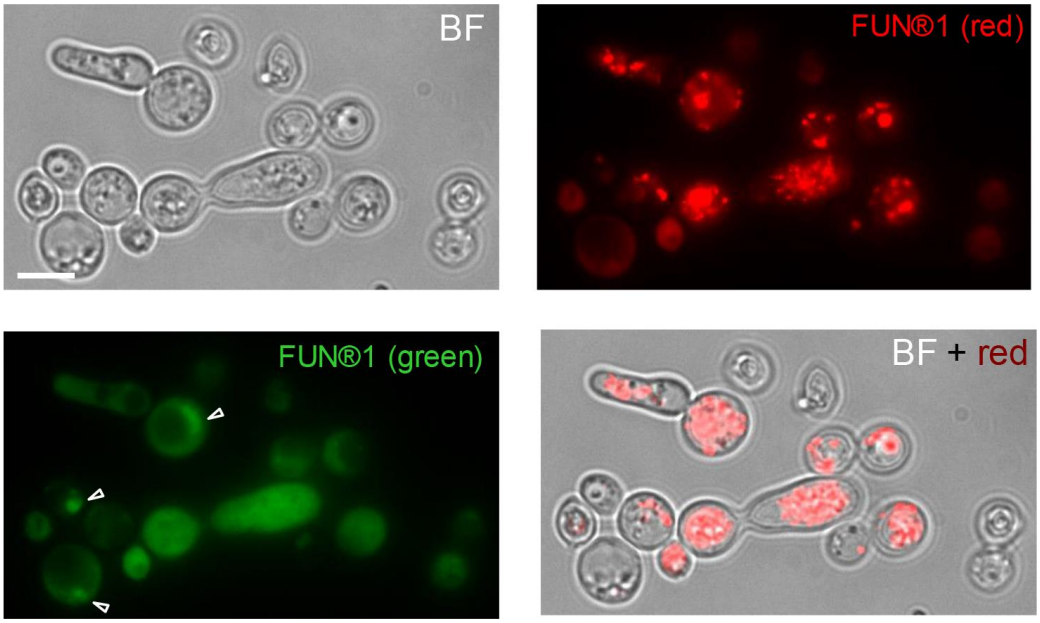

Supplementary Figure 4. Examples of *top2-5* cells stained with the vitality marker FUN® 1 after 24 h at 37 °C. Related to Figure 3C. In the green channel, hollow arrowheads point to the H2A-GFP signal. The cytoplasmic signal comes from unmetabolized FUN® 1. The brilliant aggregates in the red channel are metabolized FUN® 1 in cell bodies that retained a high vitality. Scale bar depicts 5 μm; BF, bright field.

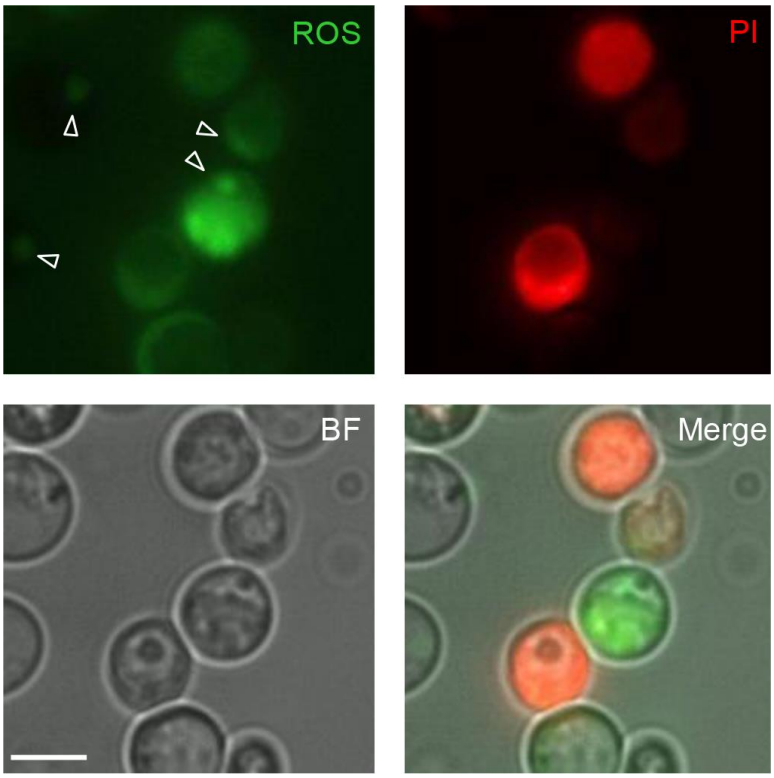

Supplementary Figure 5. Examples of *top2-5* cells co-stained for ROS and death after 24 h at 37 °C. Related to Figure 3C. In the green channel, hollow arrowheads point to the H2A-GFP signal. The cytoplasmic signal comes from ROS as reported with the DCFH-CA marker. The PI marker only stain cells that have lost plasma membrane impermeability (i.e., death cells). Note that cells are classified as ROS+ if they are bright green and PI negative. Scale bar depicts 5 μm; BF, bright field.

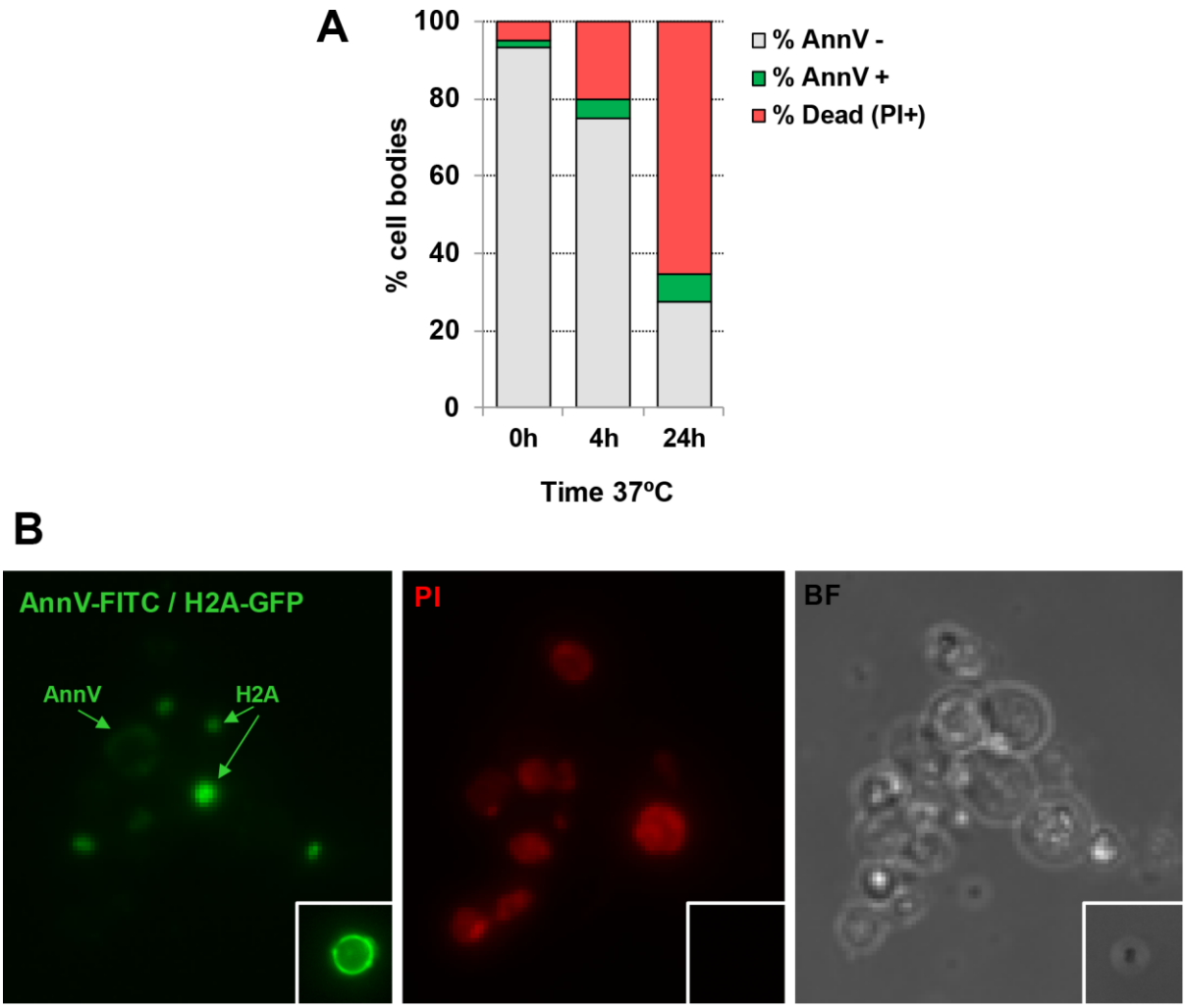

Supplementary Figure 6. Distribution of annexin V (annV) and propidium iodide (PI) co-staining in the *top2-5* population after incubation at 37 ºC. (**A**) Percentage of cell bodies with different co-staining patterns at 0, 4 and 24 h at 37 ºC. (**B**) Examples of cell bodies with different co-staining patterns at 24 h. Note that cells also carry nuclear H2A labelled with GFP. Cell bodies were classified as AnnV+ when the fluorescent green signal was seen at the body periphery (as indicated). The inlet field depicts a cell membranous subparticle (probably an organelle) strongly stained by annexin V-FITC. These unusual examples (<1% of "bodies") were not considered in the quantification since a proper cell body was not inferred in the BF. Scale bar depicts 5 μm; BF, bright field.

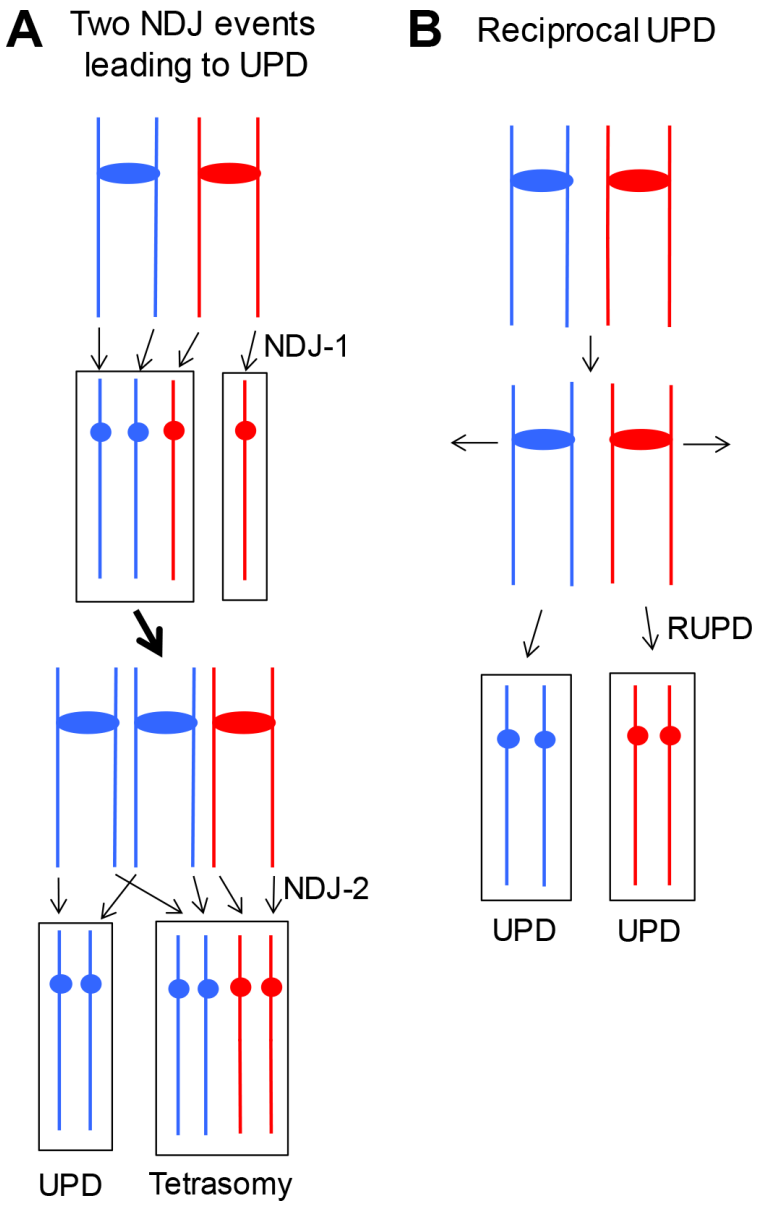

Supplementary Figure 7. Two pathways for generating UPD. (**A**) Two non-disjunction (NDJ) events in different cell cycles can result in UPD. NDJ-1 results in one trisomic strain and one monosomic strain. If a second NDJ event occurs in the trisomic strain, a UPD isolate can be generated. (**B**) Reciprocal UPD. By this mechanism, two NDJ events in the same cell cycle results in two daughter cells with reciprocal patterns of UPD.

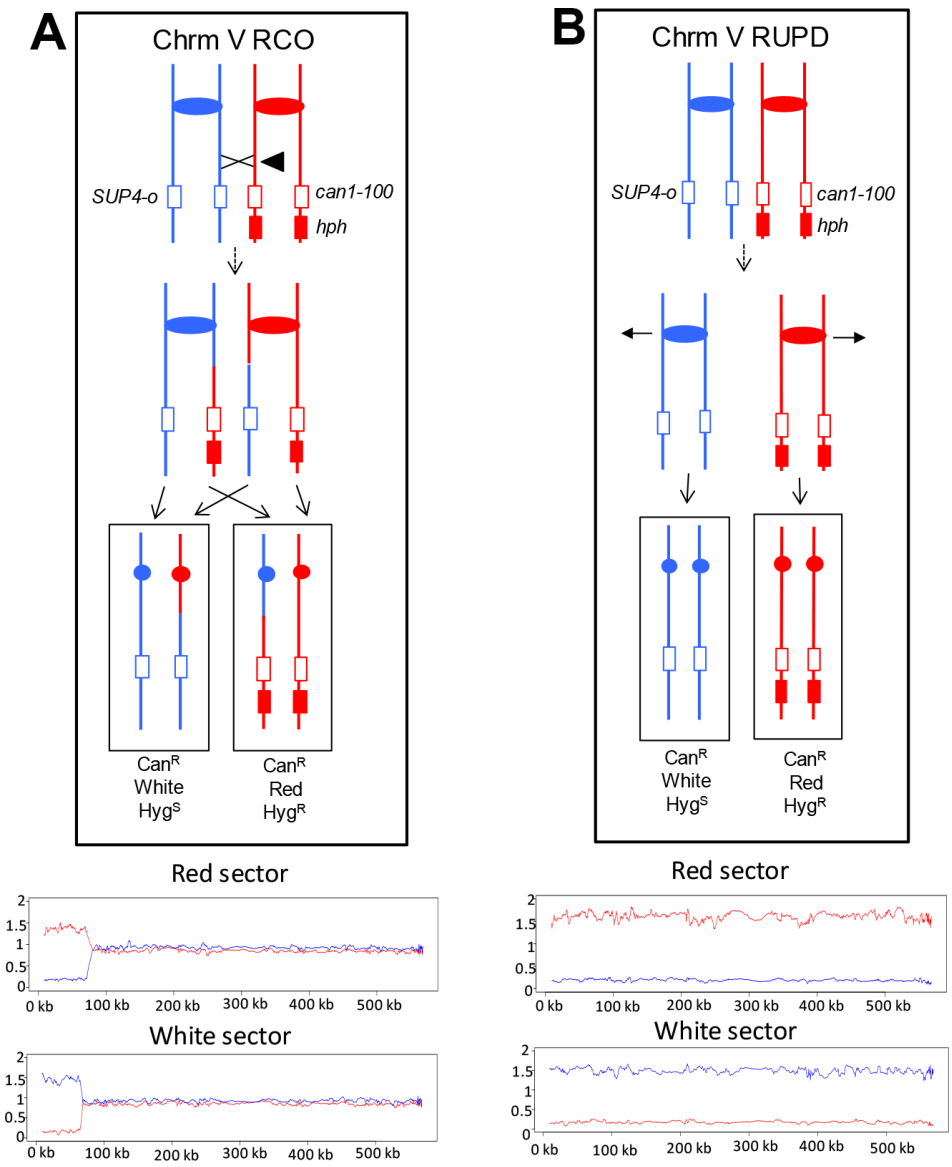

Supplementary Figure 8. Detection and analysis of reciprocal crossovers (RCO) and reciprocal UPD (RUPD). The chromosome V homolog derived from YJM789 (shown in blue) has a *SUP4-o* gene (encoding an ochre suppressor) replacing the *CAN1* gene. On the W303-1A-derived homolog, chromosome V has the ochre-suppressible *can1-100* allele with the *hph* gene (resulting in hygromycin resistance) located centromere-distal to *can1-100*. In addition, the strain is homozygous for the ochre-suppressible *ade2-1* allele; diploids with this gene and 0, 1, or 2 copies of *SUP4-o* form red, pink or white colonies, respectively. Diploids without a genetic alteration form pink, canavanine-sensitive, hygromycin-resistant colonies. (**A**) A reciprocal crossover between the *can1-100* marker and *CEN5* can result in a red/white Can^R sectored colony in which the white sector is sensitive to hygromycin. In the microarray pictures shown below the recombination event (FM1873-14 (E2) in Supplementary Table 2), hybridization values for chromosome V from the red and white sectors are shown on the top and bottom panels, respectively, at the bottom of the figure. (**B**) A reciprocal UPD event on chromosome V would be expected to produce a red/white Can^R sectored colony with the phenotypes identical to the RCO. The microarray patterns in each sector would be different. Microarrays derived from the red and white sectors of MD684.1.15 (E2) (Supplementary Table 2) are shown in the top and bottom panels, respectively, at the bottom of the figure.

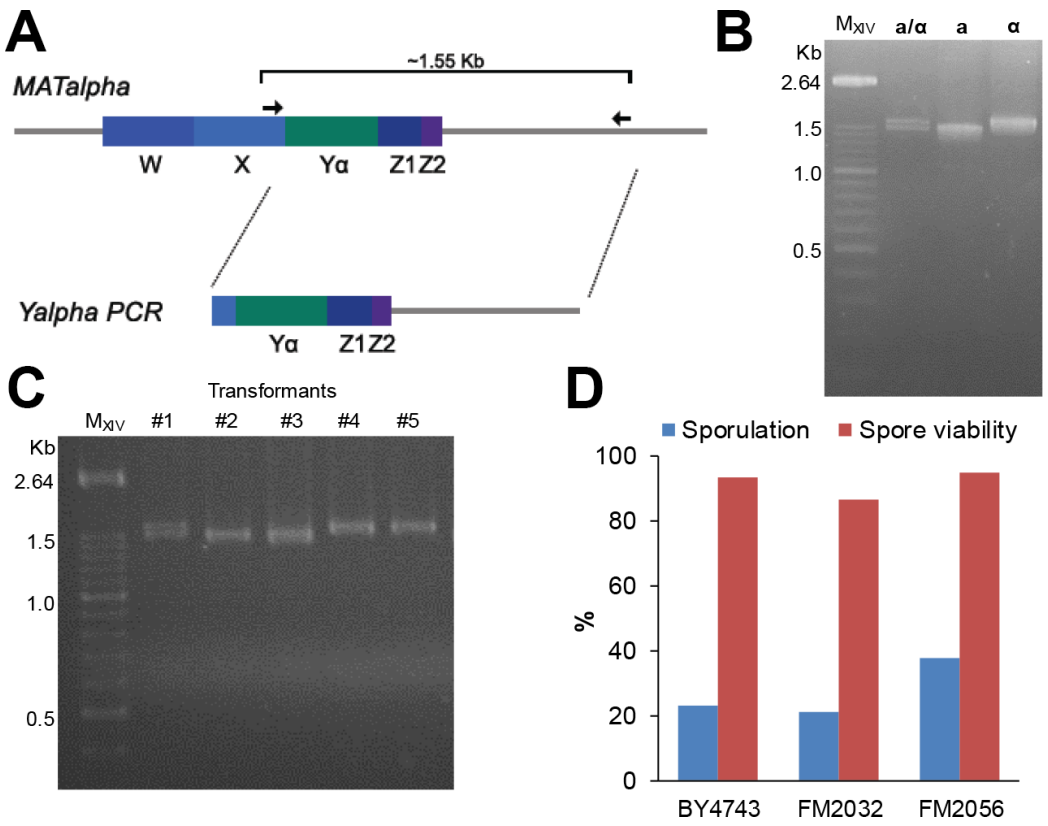

Supplementary Figure 9. One-step marker-free diploidization of *MAT*a *bar1Δ* strains. Proof of concept. (**A**) Schematic of the *MAT*α locus and the PCR-based strategy to obtain the *MAT*a-to-*MAT*α transformation product. The haploids *MAT*a and *MAT*α differ in the Y sequence within the *MAT* locus (chromosome III), but shared flanking sequences. The Yα is ~100 bps longer than Ya (747 bps vs 642 bps). The forward primer X-reg (Supplementary Table 4) binds upstream of the Y region whereas the reverse primer MAT-R does so downstream, within the sequence adjacent to the MAT locus. Importantly, MAT-R does not bind downstream the silent *HML*α and *HMR*a loci present in the same chromosome, which act during the mating type switching as template sequences for gene conversion at *MAT* [7]. (**B**) Gel separation of the three types of X-reg/MAT-R PCR products. The resulting PCR product is ~1.55 Kbps if the strain is a haploid *MAT*α, whereas it is ~1.45 kb if the strain is a haploid *MAT*a strain. A diploid would yield a double band that can be resolved in a 2% agarose gel. In these examples, the haploids and the diploid are the widely used S288C reference strains BY4741, BY4742 and BY4743. (**C**) Testing transformants for the one-step marker-free diploidization of *MAT*a *bar1*Δ strains. Only *MAT*a strains respond to the α-factor pheromone with a transient G1 arrest. The arrest is relieved by the Bar1 protease, which degrades α-factor extracelullarly. Knock-out mutants for *BAR1* become highly hypersensitive to α-factor; hence, in *bar1*Δ strains, α-factor can be used for the selection against the haploid *MAT*a genotype. In this example, competent cells from the strain FM1932 (BY4741; *MAT*a Δ*bar1::URA3*) were transformed with the Yα PCR product and spread onto YPD plates supplemented with 5 μg α-factor (spread on the plate surface). Five colonies were picked, re-struck onto YPD α-factor plates, and their genomic DNA tested for the genomic content at the MAT locus by X-reg/MAT-R PCR. Note that clone #1 is a diploid and clones #4 and #5 have become haploid *MAT*α. Clones #2 and #3 were still haploid *MAT*a. These strains probably come from spontaneous resistance to α-factor unrelated to genetic changes in the MAT locus (from our estimation: 0.2% over viable CFUs in a mock transformation experiment). (**D**) Sporulation efficiency and spore viability of the diploid obtained through the one-step marker-free method in comparison to diploids obtained through mating. BY4743 (*MAT*a/α *BAR1*/*BAR1*); FM2032 (control *MAT*a/α *bar1*Δ/*bar1*Δ obtained by mating the corresponding *bar1*Δ haploids); FM2056 (clone #1 from panel C).

Supplementary Tables

Supplementary Table 1. P-value of cross comparisons between the number of cell bodies generated after the 37 °C for 6 h → 25 ºC for 16 h regime.

Strain/condition	Microcolonies of ≥2 cell bodies at 37 ºC (N)	Microcolonies that rebudded after 25 ºC downshift (N)	P-value against *top2-5* (first row)
top2-5	160	26	-
top2-5 (Sorb)	89	21	0.1064
*top2-5 yca1*Δ	152	35	0.086
top2-5/top2-5	90	42	< 0.0001

Comparison between microcolonies of ≥2 cell bodies after the 37 °C incubation and re-budding (for at least one cell body) after the 25 °C downshift were performed in 2×2 contingency tables using a one-tailed Fisher's exact test.

Supplementary Table 2. Summary of chromosome V events in R HygR/W HygS sectored colonies of FM1873 and MD684 strains.

Strain name[1] and sector pattern[2]	Genomic alterations[3]
FM1873-1 (E2) R Hyg^R/P-W Hyg^S	UPD on V in "correct" direction in red sector; partial UPD in "incorrect" direction on V in white sector.
FM1873-2 (E2) R Hyg^R/W Hyg^S	UPD on V in "correct" direction in red sector; T-LOH on V in "correct" direction in white sector.
FM1873-4 (E2) R Hyg^R/W Hyg^S	RCO on V. Breakpoint at 134 kb in red sector and 144 kb in white sector.
FM1873-12 (E2) R Hyg^R/W Hyg^S	RUPD on V.
FM1873-14 (E2) R Hyg^R/W Hyg^S	RCO on V. Breakpoint at 67 kb in red sector and 76 kb in white sector.
FM1873-26 (E2) R Hyg^R/W Hyg^S	UPD in correct direction on V in red sector; T-LOH event in correct direction in white sector.
FM1873-32 (E2) R Hyg^R/P Hyg^S	RUPD on V
FM1873-35 (E2) R Hyg^R/P Hyg^S	RUPD on V
FM1873-37 (E2) R Hyg^R/P Hyg^S	RUPD on V
FM1873-41 (E2) R Hyg^R/P Hyg^S	RUPD on V
FM1873-45 (E2) R Hyg^R/P Hyg^S	UPD on V in the correct direction in the red sector (two copies of W303-1A-derived chromosome; white sector has one copy of YJM789-derived homolog and none of W303-1A-derived homolog
FM1873-49 (E2) R Hyg^R/P Hyg^S	No obvious changes on V in red sector; white sector has UPD on V in correct direction.
FM1873-50 (E2) R Hyg^R/P Hyg^S	RUPD on V
FM1873-54 (E2) R Hyg^R/P Hyg^S	RUPD on V
FM1873-70 (E2) R Hyg^R/P Hyg^S	RUPD on V
FM1873-85 (E2) R Hyg^R/P Hyg^S	RUPD on V
FM1873-101 (E2) R Hyg^R/P Hyg^S	RCO on V. Breakpoints at 95 kb and 86 kb in red sector. The red sector has event indicative of a G1-associated DSB, repaired in G2. Breakpoint at 93 kb in white sector.
FM1873-105 (E2) R Hyg^R/P Hyg^S	RUPD on V.
FM1873-106 (E2) R Hyg^R/P Hyg^S	RUPD on V.
FM1873-112 (E2) R Hyg^R/P Hyg^S	RUPD on V.
FM1873-1 (C2)	UPD on V in "correct" direction in red sector; partial UPD in "incorrect" direction on V in white sector.
FM1873-2 (C2)	UPD on V in "correct" direction in red sector; no clear event on V in white sector.
FM1873-3 (C2)	No detectable events on V.
FM1873-7 (C2)	No detectable events on V in red sector. In white sector, V has terminal LOH (about 110 kb).
FM1873-14 (C2)	RUPD on V.
FM1873-19 (C2)	UPD on V in red sector; no obvious change on V in white sector.

FM1873-20 (C2)	RUPD on V.
MD684.1.15 (E2)	RUPD (V)
MD684.1.17 (E2)	RUPD (V)
MD684.1.49 (E2)	RUPD (V)
MD684.1.61 (E2)	Red sector looked like haploid strain (all homologs derived from W303-1A with elevated signal, all derived from YJM789 with reduced signal. UPD on V in white sector
MD684.1.65 (E2)	Red sector looked like haploid strain (all homologs derived from W303-1A with elevated signal, all derived from YJM789 with reduced signal). In white sector: UPD on V
MD684.1.73 (E2)	Red sector looked like haploid strain (all homologs derived from W303-1A with elevated signal, all derived from YJM789 with reduced signal). In white sector: UPD on V
MD684.1.75 (E2)	Red sector looked like haploid strain (all homologs derived from W303-1A with elevated signal, all derived from YJM789 with reduced signal). In white sector, UPD on V.
MD684.1.83 (E2)	RUPD (V)
MD684.1.88 (E2)	Red sector looked like haploid strain (all homologs derived from W303-1A with elevated signal, all derived from YJM789 with reduced signal). In white sector, T-LOH on V (breakpoint at 56 kb).

[1] Parentheses after the strain name indicate whether the strain was experimental (E2, incubated for six hours at 37 ºC in liquid) or control (C2, not incubated at the restrictive temperature).

[2] Strains either treated at 37 ºC for six hours (E) or untreated (C) at the restrictive temperature were plated on solid medium containing canavanine. After colonies were formed, we purified cells derived from red and white sectors, and determined whether cells from these sectors were Hyg^R or Hyg^S (as indicated in the table). The *hph* marker was located distal to *can1-100* on the W303-1A-derived chromosome. Thus, a reciprocal crossover (RCO) or reciprocal UPD event would be expected to produce a hygromycin-resistant red sector, and a hygromycin-sensitive white sector. Code: T-LOH (terminal LOH event), I-LOH (interstitial LOH event), Tri (trisomy), UPD (uniparental disomy), RCO (reciprocal crossover), and RUPD (reciprocal uniparental disomy).

[3] The arrays for sectored colonies were done with arrays that had dense SNPs for chromosomes I, III, V and VIII, but few SNPs on other chromosomes. Thus, we tabulate only events involving chromosome V.

Supplementary Table 3. Strains used in this work.

Strain name	Relevant genotype[a]	Origin
CH326	(S288C) *MAT*a *ura3-52 his4-539am lys2-801am SUC2+ top2-5*	D. Botstein[b]
CH335	(S288C) *MAT*a *ura3-52 his4-539am lys2-801am SUC2+ TOP2*	D. Botstein[b]
FM1386	CH326; *H2A2(YBL003c):GFP:BleMX*; Δ*bar1::URA3*	F. Machin[c]
FM1419[e]	CH335; *H2A2(YBL003c):GFP:BleMX*; Δ*bar1::URA3*	F. Machin[c]
FM1856	FM1386; Δ*yca1::kanMX4*	This work
FM1871[e]	FM1419; Δ*yca1::kanMX4*	This work
FM1730[f]	*MAT*a/α *top2-5/top2-5* homozygous diploid (from FM1386)	This work
FM1732[e,f]	*MAT*a/α *TOP2/TOP2* homozygous diploid (from FM1419)	This work
PSL2	(W303a) *MAT*a *ade2-1 can1-100 his3-11,15 ura3-1 trp1-1 V9229::HYG V261553::LEU2 RAD5*	T. Petes[d]
PSL5	(YJM789) *MAT*α *ade2-1 ura3 can1*Δ*::SUP4-o gal2 ho::hisG*	T. Petes[d]
FM1830[g]	PSL2; *top2-5:9myc:natMX* (1-2 x cXIV)	This work
FM1832	PSL5; *top2-5:9myc:natMX*	This work
FM1873[g]	(FM1830 x FM1832) *MAT*a/α *top2-5/top2-5* hybrid diploid (3-4 x cXIV, cXIIr t-LOH)	This work
FM2010	(PSL2 x PSL5) *MAT*a/α *TOP2/TOP2* hybrid diploid	This work
MD681	PSL2 *top2-5:9myc:natMX* (FM1830 backcrossed with W303 to have 1 x cXIV)	This work
MD684	(MD681 x FM1832) *MAT*a/α *top2-5/top2-5* hybrid diploid (3-4 x cXIV)	This work
BY4743	*MAT*a/α *his3*Δ*1/his3*Δ*1 leu2*Δ*0/leu2*Δ*0 met15*Δ*0/MET15 LYS2/lys2*Δ*0 ura3*Δ*0/ura3*Δ*0*	Euroscarf collection
FM1932	(BY4741) *MAT*a *his3*Δ*1 leu2*Δ*0 met15*Δ*0 ura3*Δ*0*; Δ*bar1::URA3*	This work
FM1982	(BY4742) *MAT*a *his3*Δ*1 leu2*Δ*0 lys2*Δ*0 ura3*Δ*0*; Δ*bar1::URA3*	This work
FM2032	(FM1932 x 1982) *MAT*a/α *bar1*Δ/*bar1*Δ	This work
FM2056[f]	(clone #1 in Supplementary Figure9C) *MAT*a/α *bar1*Δ/*bar1*Δ (from FM1932)	This work

[a] Semicolons separate independent transformation events during strain construction. Intermediate strains are omitted.
[b] Described in [8]
[c] Described in [5]
[d] Described in [3]
[e] These strains were used as *TOP2* controls during clonogenic assays (n=3 independent experiments). In all cases, 100% viability was maintained after 0, 3, 6, 9, 12, 24 and 48 h incubations at 37 ºC.
[f] These homozygous diploids were made through the one-step marker-free transformation-based protocol described in Supplementary Figure 9.
[g] These strains were shown by SNP and copy number arrays to carry the genome alteration shown between brackets. For instance, the hybrid heterozygous *top2-5/top2-5* diploid FM1873 carried two genome rearrangements when compared to its isogenic *TOP2/TOP2* counterpart: 3-4 copies of cXIV and a t-LOH at cXII right arm.

Supplementary Table 4. Primers used in this study.

Primer name	Purpose	Sequence (5′ to 3′)
Yca1-F (-359)	To amplify Δ*yca1::kanMX* from gDNA	CAATGCATTGGATCTTATTGGC
Yca1-R (+1709)	To amplify Δ*yca1::kanMX* from gDNA	GTCGAAACAAGAAGAGCAAAC
Bar1-F (-196)	To amplify Δ*bar1::URA3* from gDNA	GCCAGCTATTCTGAAACACACCAC
Bar1-R (+2316)	To amplify Δ*bar1::URA3* from gDNA	AACAGTCTTAGGGAAGTAACGAG
Top2-S3	To tag *TOP2* at 3' with *9xmyc:natMX*	GGAAAACCAAGGATCAGATGTTTCGTTCAAT GAAGAGGATCGTACGCTGCAGGTCGAC
Top2-S2	To tag *TOP2* at 3' with *9xmyc:natMX*	TATAAAAAGAATGGCGCTTTCTCGGATAAAT ATTATTCAATCGATGAATTCGAGCTCG
Top2-F (-175)	To amplify top2-5*:9xmyc:natMX* from gDNA	AAGACGCGCCAGTAGGACGC
Top2-R (+4511)	To amplify top2-5*:9xmyc:natMX* from gDNA	CGCACGATGTTTTTCGCCCAGG
Xreg-F	To amplify Yα region in the MAT locus (Yα transformation product)	TTGTTGGCCCTAGATAAGAA
MAT-R (+2894)	To amplify the MAT locus (Yα transformation product)	CAAGGGAGAGAAGACTTGTG

Supplementary Table 5. Landscape of possible outcomes during microcolony experiments.

After 37 ºC (Top2 inactivation)	After 25 ºC reincubation (Top2 re-activation)
0 (lysis)	---
1 (did not bud)	0 (lysis) 1 (remained unbudded) 2 (able to bud once Top2 is back) 3, 4, 5, etc. (short-term budding capability) >20-50 (will raise a viable population)
2 (did bud once without Top2)	0 (double lysis) 1 (one body lysed; the other did not divide again) 2 (no more budding even after Top2 reactivation) 3 (one body able to bud once Top2 is back) 4, 5, etc. (both bodies able to bud*) >20-50 (at least one body/cell is viable)
3 (did bud twice without Top2)	0, 1, 2 (no more budding and some bodies lysed) 3 (no more budding even after Top2 reactivation) 4 (1 of 3 bodies rebudded once) 5 (2 of 3 bodies rebudded once*) 6, etc. (3 of 3 bodies rebudded once *) >20-50 (at least one body/cell is viable)
4 (mother and daughter rebudded again*)	0, 1, 2, 3 (no more budding and some bodies lysed) 4 (no more budding even after Top2 reactivation) 5, 6, 7, 8, 9 (1-4 of 4 bodies rebudded once*) >20-50 (at least one body/cell is viable)
Etc.	Etc.

* Other interpretations on the origin of these microcolonies are possible.